Journal of Nuclear Materials 394 (2009) 67–86

Contents lists available at ScienceDirect

Journal of Nuclear Materials

journal homepage: www.elsevier.com/locate/jnucmat

Overview of high-temperature fuel behaviour with relevance to CANDU fuel

B.J. Lewis [a,*], F.C. Iglesias [b], R.S. Dickson [c], A. Williams [c]

[a] Royal Military College of Canada, P.O. Box 17000, Kingston, Ontario, Canada K7K 7B4
[b] Candesco Corporation, 230 Richmond Street, 10th Floor, Toronto, Ontario, Canada M5V 1V6
[c] Atomic Energy of Canada Limited – Chalk River Laboratories, Chalk River, Ontario, Canada K0J 1J0

ARTICLE INFO

Article history:
Received 4 May 2009
Accepted 11 August 2009

ABSTRACT

This paper provides an overview of high-temperature phenomena in nuclear fuel elements and bundles, with particular relevance to the CANDU fuel design. The paper describes heat generation, fuel thermal response, and thermophysical properties of the fuel and sheath that can affect the thermal and mechanical response of the fuel element. Sources of chemical heat that can arise during accident conditions in the fuel element are also detailed. Specific phenomena associated with fuel restructuring, fuel sheath deformation, fuel-to-sheath heat transfer, fuel sheath failure criteria, oxidation, hydriding and embrittlement of the Zircaloy sheath, gap transport processes in failed elements, fuel/sheath interaction and fuel dissolution by molten cladding are detailed as important phenomena that can impact reactor safety analysis. Fuel behaviour during a power pulse and fuel bundle behaviour that occurs during a severe reactor accident are further considered. The review also points out areas of further research that are needed for a more complete understanding.

1. Introduction

The prediction of high-temperature fuel behaviour is of particular importance for nuclear safety analysis. An understanding of fuel behaviour has been well advanced through many decades of experimental research and efforts in modelling and code development [1]. Various types of component and system computer codes have been developed by the international fuel community to describe fuel behaviour and performance during normal, upset and severe accident conditions [2–11]. In Canada, the ELESTRES code has been developed for the prediction of fuel performance during normal operating (steady-state) conditions [12,13], and the ELOCA code for upset/transient conditions [14,15]. These various codes describe the complex and linked phenomena associated with the thermo-mechanical and chemical behaviour of the fuel rod/bundle.

An overview of experimental programs on core melt progression in light water reactors (LWR) and the associated fission-product release behaviour has been previously detailed [16]. The current work provides an overview of phenomena that can arise in nuclear fuel during high-temperature conditions. In particular, this paper addresses the thermophysical properties, fuel restructuring mechanisms and heat transfer considerations that must be known for the simulation of nuclear fuel performance during normal operation and for transient conditions that may arise during a postulated reactor accident. It also focuses on the thermal and mechanical behaviour of the fuel element during high-temperature conditions that can lead to sheath failure. In addition, this work details chemical effects of oxidation and hydriding of the sheath, as well as fuel dissolution effects that can lead to severe fuel deformation. These various phenomena are discussed in relevance to the CANada Deuterium Uranium (CANDU) fuel element/fuel bundle design.

2. Phenomena review

2.1. Fuel element behaviour parameters

2.1.1. Heat generation in a fuel element

The flux depression that occurs across the fuel element radius is due to the effect of neutron absorption, primarily by the major fuel constituent of ^{238}U atoms and the distribution of fissile atoms. With burnup, resonance absorption in the ^{238}U leads to a buildup of ^{239}Pu near the pellet surface, which affects the fission density distribution that can be approximated as [17,18]:

$$H(r) = H(0)\ \{\mathrm{I}_o(\kappa r) + \beta\ \exp[\lambda(r-a)]\} \quad (1)$$

where $H(r)$ is the volumetric heat generation rate at the radial position, r, in the pellet, κ and λ are the inverse neutron diffusion lengths for neutrons in the pellet and in the pellet surface layer, respectively, I_o is the modified Bessel function of first kind of order zero, β is the fractional increase in heat production at the pellet surface due to fissile atom buildup and a is the pellet radius. Fuel performance codes do not take into account any redistribution of

* Corresponding author. Tel.: +1 613 541 6611; fax: +1 613 542 9489.
E-mail address: lewis_b@rmc.ca (B.J. Lewis).

0022-3115/$ - see front matter Crown Copyright © 2009 Published by Elsevier B.V. All rights reserved.
doi:10.1016/j.jnucmat.2009.08.011

(volatile) fission products that can absorb neutrons (e.g. ^{135}Xe), although this effect is expected to be negligible due to the much larger quantity of fertile and fissile material present in the fuel.

In general, most modern fuel performance codes use more detailed models to determine the radial profile of the heat generation rate, such as those described by Lassmann et al. [19,20]. These models are based on detailed neutron diffusion calculations, and take into account the changing concentrations of the U, and Pu isotopes, and are hence capable of accounting for the change in the profile as a function of burnup.

2.1.1.1. End flux peaking. For a given neutron flux level in the vicinity of a fuel bundle, local flux variations occur due to the absorption of neutrons by the fuel and the local change in the fissile material composition. End flux peaking occurs at the ends of the bundle, where there is an absence of neutron attenuating material because of the small cross section of the Zircaloy components (i.e. the flux increases by a factor of ~2 at the end of the fuel bundle) [21]. This higher local neutron flux produces a slightly higher heat generation rate in the end pellets as compared to the midplane of the fuel element. The flux changes as a function of the distance from the fuel element midplane have been measured in the ZED-2 zero power facility at the Chalk River Laboratories [22]. Modelling of the end flux peaking phenomenon has been performed, and predictions have been shown to be within experimental error [23].

Fuel element end caps provide an additional surface area for axial heat transfer from the end pellets as well as the sheath by axial heat conduction. The advantage of the increased heat transfer at the end of the elements is offset by the increased local heat generation caused by end flux peaking. During normal operation, end flux peaking can provide an extra source of heat in the end cap region which can influence the local temperature [24]. For reactor accidents in which the temperatures are high enough to reduce safety margins, heat transfer to the end cap is an important consideration.

2.1.2. Fuel thermal properties

For transient analysis, a solution of a time-dependent heat conduction equation is required:

$$\rho Cp \frac{\partial}{\partial t} T = \nabla \cdot [k \nabla T] + H \tag{2}$$

where T is the fuel temperature, k is the fuel thermal conductivity, H is the volumetric heat generation rate, ρ is the fuel density, C_p is the specific heat capacity of the fuel and t is the time. Thus, to model the high-temperature fuel behaviour, the following fuel material properties are needed for fresh, irradiated and oxidized uranium dioxide fuel:

- Thermal conductivity.
- Specific heat capacity.
- Thermal expansion.
- Fuel melting temperature.

There have been a number of extensive reviews of fuel thermal properties. For instance, correlations proposed in the MATPRO materials handbook, which can be used in fuel rod performance codes for normal and reactor accident analysis, are derived from an extensive literature review of experimental data [25–28]. A report on thermophysical properties was also prepared in 1997 by an International Working Group of the International Atomic Energy Agency where available data and correlations were compiled for materials of light and heavy water-cooled reactors [29]. A comprehensive and critical review of the thermophysical properties for uranium dioxide has been presented more recently by Fink [30], as well as for both UO_2 and mixed-oxide (MOX) fuels by Carbajo et al. [31]. A brief review of the thermal properties required for Eq. (2) is given below.

(i) Thermal conductivity

Correlations are normally required for the thermal conductivity as a function of temperature, composition and deviations from stoichiometry. Early correlations for UO_2 from 273 to 3113 K are given as a function of temperature and porosity in MATPRO [25]. In a later version of MATPRO [27], the fuel thermal conductivity is provided as a function of temperature, density, oxygen-to-metal (O/M) ratio (based on a simple model suggested by Olander [32]) and plutonium content of the fuel. The MATPRO correlation has been further improved by accounting for the effects of fuel burnup using the 1992 correlation of Lucuta et al. [28,33].

The thermal conductivity expression proposed by Harding and Martin accounts for the phonon and small polaron contributions for uranium dioxide as a function of temperature between 773 and 3120 K [34]. This correlation has been widely used in computer codes or as the basis for other correlations. The work of Lucuta et al. is of particular importance because it separated the different effects of burnup, radiation and deviation from stoichiometry by using SIMFUEL that allows a simulation of burnup with the supplement of stable additives to the UO_2 fuel matrix [35]. In the correlation of Lucuta et al., the Harding and Martin formula for fully dense, unirradiated fuel (λ_0) is multiplied by five factors that account for the effects of dissolved fission products (κ_{1d}), precipitated solid fission products (κ_{1p}), porosity from pores and fission gas bubbles (κ_{2p}), deviation from stoichiometry (κ_{3x}) and radiation damage (increase in lattice defects) (κ_{4r}) (i.e. as a correlation up to a temperature of 1900 K):

$$\lambda = \kappa_{1d}\kappa_{1p}\kappa_{2p}\kappa_{3x}\kappa_{4r}\lambda_0 \tag{3}$$

The fuel thermal conductivity model used in both the ELESTRES and ELOCA 2.2 codes is based on a variation of this model. The factor for the deviation from stoichiometry is assigned a value of unity under typical conditions of burnup with intact fuel (since the fuel is not expected to deviate much from stoichiometry). However, for fuel with defects or under accident conditions, Lucuta et al. suggest that the Harding and Martin formula can be replaced by a lattice expression as derived from UO_{2+x} and hyperstoichiometric SIMFUEL data (i.e. Eq. (13) of Ref. [35]) for stoichiometry deviations up to 0.1. This nonstoichiometry correlation is consistent with a similar one proposed by Goldsmith and Douglas in the temperature range 670–1270 K [36].

Based on the Halden Research Project with fuel instrumented with thermocouples for temperature measurement, Wiesenack et al. developed a simple formula for irradiated UO_2 of 95% theoretical density (TD) up to a burnup of 67 MWd/kgU that only depended on the two variables of fuel temperature and burnup [37,38]. The Halden measurements for irradiated fuel indicate a larger reduction in thermal conductivity than that suggested for SIMFUEL and therefore the Lucuta et al. correlation may underestimate the effect of burnup (especially at higher burnups as experienced by light water reactor fuel).

In 1999, Ronchi obtained new experimental data of the thermal conductivity from the simultaneous measurement of the heat capacity and thermal diffusivity and developed a correlation up to 2900 K with terms for the phonon lattice and ambipolar contribution [39]. The phonon contribution is generally dominant and results from the scattering of phonons with lattice defects and phonon self-scattering for temperatures below 3000 K. In 2000, Fink proposed a new correlation in better agreement with available data using the ambipolar term of Ronchi and an improved lattice term [30]. Finally, the effects of burnup on the thermal conductivity of uranium dioxide, which include soluble fission products, irradiation-induced point defects and extended defects such as

microbubbles, was investigated by Amaya et al. in 1997 [40], and most recently studied by Ronchi in 2004 (up to a burnup of 100 GWd t^{-1}) [41]. In the 2004 Ronchi analysis, a complicated treatment was suggested that takes into consideration the relevant effects and structural changes induced by reactor burnup, including the recovery of thermal conductivity as a function of temperature (i.e. as derived from laboratory annealing experiments up to 1450 K), and the separate effects of soluble fission products, fission gas frozen in dynamical solution and radiation damage.

Most treatments do not account for changes in stoichiometry, which is particularly important for defected fuel analysis since hyperstoichiometric fuel has a reduced thermal conductivity. In addition, there is also a reduction in the incipient melting temperature for hyperstoichiometric fuel (see item iv).

The stoichiometry effect has been addressed most recently following the analysis in Refs. [42–46]. For instance, the parameter $\lambda_0\kappa_{3x}$ in Eq. (3) can be replaced by the factor $\lambda_0(T,x)$ ($=\lambda_{AP}+\lambda_L$) which is composed of the original ambipolar term λ_{AP} proposed by Ronchi in 1999 (i.e. Eq. (8) of Ref. [39] corrected to 100% TD) and a term which accounts for the lattice defects λ_L ($=[A(x)+B(x)T]^{-1}$) based on the correlation proposed by Ellis, Porter and Shaw (EPS) in 2000 for unirradiated UO_{2+x} [47], as derived from available literature data in Refs. [48–54]. In fact, the same treatment for hyperstoichiometric and irradiated fuel has been recommended by Carbajo et al., except that the correlation of Luctua et al. for nonstoichiometric fuel (i.e. Eq. (13) in Ref. [35]) is suggested in place of the EPS correlation for λ_L. Alternatively, the thermal conductivity model of Amaya et al. [55] has been used instead in the defective fuel analysis of Ref. [46]. This latter model is consistent with experimental data of thermal conductivity in UO_{2+x} over a wide range of temperature (300–1400 K) and stoichiometry ($x < 0.2$).

Shaw et al. carried out experiments to measure the thermal diffusivity on both oxidized and irradiated urania fuel up to 1173 K, where irradiated fuel samples were subjected to a low temperature anneal in air at 733 K to oxidize the samples [56]. However, a recovery was seen on progressively heating the samples to higher temperatures than that previously attained. This result suggests that the laboratory procedure to manufacture oxidized samples of irradiated fuel material may not be representative of actual in-pile (defect) conditions. As mentioned, the effects of recovery for (stoichiometric) irradiated material were investigated in the recent experiments of Ronchi et al. [41]. Typically, the experimental uncertainty in most of the literature data for the diffusivity and heat capacity is, respectively, 10–15% and 20–30% [39].

For liquid UO_2 fuel, a value of 2.5 ± 1 W m^{-1} K^{-1} has been recommended by both Fink and Carbajo et al. [30,31].

Thermal conductivity data on UO_2 doped with lanthanide burnable poisons (Dy or Gd) are of interest in CANDU fuel development for low void reactivity fuel (LVRF), while data for hyperstoichiometry and hypostoichiometric fuel ($UO_{2\pm x}$) are useful for analysis under accident conditions after the sheath has defected, or the fuel is undergoing UO_2/Zircaloy interaction or reduction by hydrogen-rich environments (see Section 2.4). In general, although there is a large quantity of data for unirradiated uranium dioxide fuel over a wide temperature range up to fuel melting, experiments with both hyperstoichiometric and irradiated fuel are needed especially at high temperatures. There are currently no direct measurements of the thermal conductivity of hyperstoichiometric fuel at temperatures above 1770 K [48,55,57–59]. Measurements of irradiated (in-pile) uranium dioxide fuel indicate a larger reduction in thermal conductivity than that for SIMFUEL and thus a better understanding may be needed for irradiated fuel.

It is important to note that the thermal conductivity derived from the Ronchi diffusivity measurements on unirradiated fuel [41] are consistently lower than the majority of measurements reported by previous authors [28] by approximately 10%. The reason for this discrepancy is currently unexplained, and at present the Ronchi measurements have not been accepted for inclusion in fuel performance codes used by the Canadian nuclear industry.

(ii) Heat capacity

MATPRO correlations for the heat capacity for solid UO_2 follow from the original work of Kerrisk and Clifton in 1972 [25,27,60]. The MATPRO correlations have been revised so that these correlations are now a function of temperature, fuel composition (UO_2, PuO_2 and gadolinium) and oxygen-to-metal ratio [28]. Fink has developed improved correlations for the heat capacity for UO_2 accounting for the lattice phonon contribution, the thermal expansion contribution and defect formation following a review of all data in 2000 [30]. For temperatures above 2000 K, the Fink correlation is in better agreement with the 1999 high-temperature data of Ronchi [39] than the MATPRO correlation. A spike in the heat capacity, indicating a λ-phase transition as a result of an order–disorder transition in the anion sublattice has been observed for the heat capacity of UO_2 at 2670 ± 30 K by several investigators [39,61–63].

The specific heat for simulated-burnup UO_2 using SIMFUEL was measured between room temperature and 1673 K [33,48,64,65]. Here, the specific heat was observed to increase only slightly with burnup in accordance with the Kopp–Neumann rule, indicating that the influence of fission products on the heat capacity is very small.

The model for the fuel specific heat capacity used in ELOCA 2.2 employs the MATPRO 9 correlation [25] (which is the original model proposed by Kerrisk and Clifton) [60]. As mentioned, this model is a function of temperature only, where it is implicitly assumed that the fuel specific heat capacity is independent of the fuel burnup over the range of burnup experienced by CANDU fuel.

Fink has also provided the heat capacity of liquid UO_2 [30].

The correlation for heat capacity C_p (J mol^{-1} K^{-1}) developed by Kerrisk and Clifton [60] has been further generalized for hyperstoichiometric fuel [27]:

$$C_p = \frac{k_1\theta^2 e^{\theta/T}}{T^2(e^{\theta/T}-1)^2} + 2k_2T + \frac{yk_3E_a}{2T^2}e^{-E_a/T} \tag{4}$$

where T is the temperature (K), $y = 2 + x$ is the O/M ratio, $\theta = 532.285$ K, $E_a = 18968.5$ K, $k_1 = 80.1$ J mol^{-1} K^{-1}, $k_2 = 3.283 \times 10^{-3}$ J mol^{-1} K^{-2} and $k_3 = 2.361 \times 10^7$ J mol^{-1}. This model has been employed, for example, in the ELOCA-IST 2.1 code (with $y = 2$). The model in Eq. (4), however, has been refit by Fink to the higher temperature data of Ronchi yielding the slightly revised coefficients: $\theta = 548.68$ K, $E_a = 18531.7$ K, $k_1 = 81.613$ J mol^{-1} K^{-1}, $k_2 = 2.285 \times 10^{-3}$ J mol^{-1} K^{-2} and $k_3 = 2.360 \times 10^7$ J mol^{-1}, which is valid over the temperature range $298 \leqslant T \leqslant 3120$ K [30]. Matzke has further generalized Eq. (4) using SIMFUEL data to account for the effect of burnup where k_2 is multiplied by the correction factor $(1 + 0.11\beta)$ which is a function of burnup β (in atom%) [65].

A correlation for the specific heat capacity (in J mol^{-1} K^{-1}) for hyperstoichiometric UO_{2+x} as a function of the temperature T (K) and stoichiometry deviation x has also been developed from a comprehensive thermodynamic treatment of the complete uranium–oxygen system [44]:

$$\begin{aligned} C_p(x,T) = {} & 52.1743 + 45.8056x + (87.951\times10^{-3} - 7.3461\times10^{-2}x)T \\ & + (1-x)\{-84.2411\times10^{-6}T^2 + 31.542\times10^{-9}T^3 \\ & - 2.6334\times10^{-12}T^4\} - (713910 + 295090x)T^{-2} \end{aligned} \tag{5}$$

The effect of burnup (using the Matkze correction) is small. Unfortunately, there are no experimental heat capacity data available for highly-hyperstoichiometric fuel at high-temperature, where the heat capacity models mostly rely on the lower-temperature SIMFU-

EL data of Lucuta for their validation as a function of both stoichiometry and burnup [44]. Due to a lack of data, even the most recent MATPRO correlation employs the simple model of Lucuta et al. to account for the effect of fuel burnup [28].

(iii) Density

As recommended in both the reviews of Fink [30] and Carbajo et al. [31] the thermal expansion and density for solid UO_2 can be taken from the work of Martin from 273 K up to the melting point as follows from the linear thermal expansion relations in Eq. (1a) and (1b) of Ref. [66]. These correlations are for fully dense fuel and have an uncertainty of ±1% over the entire temperature range. Thermal expansion measurements on UO_{2+x} are complicated by the presence of more than one phase at low temperature. The thermal expansion of $UO_{2.00}$ lies very close to that for UO_{2+x} up to 1520 K. However, there is a lack of experimental data for hyperstoichiometric fuel above this temperature value.

The model for the fuel thermal expansion employed in ELOCA 2.2 uses the correlation proposed in MATPRO 11 (Rev. 2) [26]. This model only accounts for thermal expansion of UO_2 as a function of temperature (where burnup effects are ignored for the typical range of burnup experienced by CANDU fuel).

The recommended correlation for the density of liquid UO_2 in the temperature range 3120–4500 K is given by Breitung and Reil [67], as recommended in both the Fink and Carbajo et al. reviews.

(iv) Melting of stoichiometric and hyperstoichiometric uranium dioxide

To develop a phase diagram of the uranium–oxygen system [43,68–70], one requires a determination of the solidus and liquidus lines for hyperstoichiometric fuel. This U–O phase diagram can be used to provide the thermodynamic boundary conditions for models, which account for the fuel oxidation kinetics for fuel possibly containing a molten core [71]. In addition, a multi-component thermodynamic treatment can be further advanced to evaluate how the melting temperature would be affected with the addition of fission products and dopant material [72–74].

Recent experiments at high pressure (250 MPa) have been performed to minimize the non-congruent evaporation of urania in order to determine the solid–liquid transition in stoichiometric and hyperstoichiometric UO_2 [75–78]. The incipient melting point of hyperstoichiometric fuel decreases with increasing x, which has an impact on defected fuel performance (and the possibility of fuel centreline melting) [79].

2.1.3. Uranium dioxide restructuring and relocation

Restructuring and relocation occurs in UO_2 fuel pellets to minimize the mechanical and thermal stored energy, where a dense annular pellet forms with cracks in the colder peripheral region. The processes leading to this re-formation are detailed below [80].

(i) Porosity

Any porosity within the fuel moves in a temperature gradient towards the higher temperature region [81]. Columnar grains are formed within seconds with a movement of lenticular pores towards the hot pellet centre. The rate of pore migration in the colder outer rim of the pellet is much slower, which is on a time scale of hundreds of hours in CANDU fuel, which operates at higher linear powers up to about 60 kW m^{-1}.

The presence of porosity reduces the fuel thermal conductivity, where this effect in Eq. (3) can be described by the Loeb expression [82]:

$$k_{2p} = (1 - \beta_T P) \tag{6}$$

Here P is the porosity and the parameter β_T accounts for the temperature effect where $\beta_T = 2.6–0.5 \times 10^{-3}\, T\,(\mathrm{K})$ [30]. The porosity leads to higher fuel temperatures that promotes faster porosity elimination.

With the exception of microcracking (see item vi), porosity and its effect on thermal conductivity is simulated in the fuel modelling codes, ELESTRES and ELOCA [14]. Due to the long irradiation times involved, ELESTRES also models the dynamics of porosity change.

(ii) Sintering and densification

Oxide fuel is fabricated by pressing powdered UO_2 and sintering it at a high-temperature that is greater than one-half of the melting point. By controlling the sintering time, temperature and atmosphere, pellet densities of 95–98% of theoretical density are achieved for CANDU fuel pellets. In this process, the porosity is eliminated in the following stages [81]. The UO_2 powder fuses together at contact points to form necks, where surface forces produce more or less cylindrical tubes lying along the juncture of three or more grains. The tubular network pinches off and produces nearly spherical voids at the corners of the grains, which is essentially uniform throughout the pellet. Isolated pores can be eliminated by vacancy migration to the surrounding grain matrix; however, some residual porosity is normally maintained to accommodate swelling of fission products (see item iii).

Grain growth can occur during sintering due to the high temperatures. Voids on the grain-boundary form intergranular porosity (see item v).

Fuel densification is an important mechanism to model since fuel porosity, which is an important parameter in the fuel thermal conductivity expression, (see item i) will directly affect the fuel temperature prediction. Moreover, fuel densification will affect the gap dynamics because the thin sheath in the CANDU design (i.e. ~0.43 mm thickness) will creep down onto the fuel pellet surface due to the differential pressure between the coolant and the internal-element atmosphere during normal operation. In addition, the sheath can also lift off of the pellet surface during a Loss of Coolant Accident with coolant depressurization and any enhanced fission gas release/increased internal-element pressurization at higher fuel temperatures. Thus, to accurately model heat transfer through the fuel and the fuel-to-sheath gap, it is important to understand fuel densification effects, and any fuel expansion with solid and gaseous fission-product generation with fuel burnup. To account for fuel densification effects during operation, empirical correlations are available to account for the porosity change as a function of temperature and fuel burnup [83]. However, a more detailed model for fuel densification with irradiation has been proposed by Assmann and Stehle, which encompasses all other treatments that takes into account the behaviour of both fine and coarse pores in the fuel matrix over a range of temperature [84].

(iii) Intra-granular porosity

Intra-granular porosity remaining from fuel pellet fabrication is quickly reduced during normal reactor operation as a result of fission fragment bombardment and re-solution back into the lattice, although a population of very small pores that contain fission gas will be maintained during irradiation [85]. At decay power levels, a population of intra-granular bubbles can re-establish where the re-solution rates due to fission are low.

Fission-product gases will also diffuse from the lattice to the grain boundaries. At low fission rates and high-temperature (i.e. annealing conditions), large scale intra-granular porosity can re-form with a certain fraction of the fission-product gases in the lattice being used to re-establish the intra-granular bubble population. When conditions permit, the porosity within the fuel coarsens with irradiation as small pores coalesce to form larger pores.

Intra-granular bubbles near the grain surface can more readily lose their contents to the grain-boundary than bubbles located in the interior of the grain. Interior bubbles will migrate by surface diffusion, bulk diffusion or vapour transport. Fuel swelling has been measured for normal operating conditions and for transients up to 2270 K in various experiments with fuel swelling measure-

ments of the grain face area, number of pores, bubble density per unit area, fractional coverage, volumetric swelling due to gaseous and solid fission products, bubble coalescence, and fraction of bubbles vented to grain-edge tunnels [86–96]. The main contribution to fuel swelling under CANDU LOCA conditions arises from grain-boundary bubbles.

(iv) Columnar grain growth and central void formation

Columnar grains are formed by the movement of lenticular shaped pores (with major axes normal to the temperature gradient) up the temperature gradient at temperatures in excess of ~1700 °C with sustained temperature [81]. Cavities and small pores, pinched off from the tips of the lenticular pore, decorate the radial surfaces on these columnar grains. The migration rate is controlled either by surface diffusion or vapour transport from the hot surface to the cold surface of the pore [97].

Columnar grain growth is the primary mechanism whereby the pore volume (plus any contained and swept volatile fission products) is transported to the fuel centreline where a central hole or cavity can be formed. However, plastic flow can eliminate central voidage formed in high powered, high density fuel [98]. Thus, where the porosity has not been used to accommodate thermal expansion, plastic deformation or fission-product swelling, the porosity will migrate and agglomerate as a central void. The elimination of porosity by columnar grain growth improves the thermal conductivity of the fuel. Fuel containing a central void will have a lower central temperature than an equivalent cylindrical fuel element. The ELESTRES code simulates the effects leading to the formation of a central void and the resulting decrease in central temperature.

(v) Grain-boundary bubbles

Fission-product gases that diffuse to the grain-boundary or accumulate during grain growth as the grain-boundary sweeps through adjacent grains, collect and forms grain-boundary bubbles. As the grain-boundary bubbles grow they can touch and interlink to form saturated grain boundaries. Excess gas is vented to grain-edge bubbles or tunnels. Following a significant change in temperature over a short time interval, the saturated boundaries/tunnels can open and release their gas to the free voidage within the fuel element [97]. Based on post-irradiation annealing of boiling water reactor fuels, the fraction of the grain face area occupied by bubbles ranges from ~40% to 50% [99,100]. However, Rest has suggested that the maximum projected area coverage of the grain face by bubbles on a saturated grain-boundary is ~91% for the prediction of transient gas release with microcracking under severe accident conditions [101].

The previous description refers to grain-boundary dynamics during normal operation where heating rates are less than 250 °C/s [85]. At higher heating rates, grain-boundary bubbles can cause grain-boundary separation.

(vi) Fuel cracking and voidage

At temperatures in excess of approximately 1000 °C, UO_2 can deform plastically. If the fuel pellets are constrained by the sheath, the UO_2 can be forced to flow axially into the residual pellet dishing thus reducing the fuel element internal voidage. Thermal expansion of the hot pellet will also reduce internal fuel element voidage. Creep down of the sheath by high coolant pressure also reduces internal voidage. In general, reduction of fuel element internal voidage reduces fuel temperatures by promoting improved heat transfer paths within the fuel element. Where the fuel temperatures are too low to reduce tensile stress by plastic flow, the UO_2 will crack to relieve these stresses. Cracking and plastic deformation reduce the mechanical energy stored in the UO_2. Relocation of the fuel fragments produced by cracking also leads to reduced fuel temperatures. In the colder regions of the pellet where the fuel is more brittle, volume swelling of the grain-boundary bubbles by overpressurization can lead to crack propagation from the sharp ends of the lenticular bubble [85,102], or early interconnection of bubbles by rapid grain-boundary diffusion [103]. At very high temperatures greater than 2300 °C, grain-boundary bubbles can take the form of large spheroid gas pools [85]. Overpressurization occurs at heating rates where gas atoms arrive at the grain-boundary faster than the bubbles can grow. At very high heating rates (i.e. in excess of 5000 °C/s), energetic microcracking (or "explosive fragmentation") has been postulated (see Section 2.5) [85].

Fuel crack patterns in UO_2 pellets tend to be radial although the fracture surfaces are through weak points in the pellet and therefore a circumferential component also occurs. "Radial" cracks that are observed in cold fuel are produced during heating and cooling. Upon startup of a fresh fuel element, radial cracks are induced in the fuel pellets by circumferential thermal stresses for linear ratings in excess of approximately 7 kW/m [104]. Due to the brittle nature of UO_2 at these temperatures, these radial cracks will begin at the fuel surface and extend to the fuel pellet centreline. As the power is increased, additional radial cracks will form. As observed in CANDU fuel, the number of radial cracks is approximately equal to one-half of the linear heat rating (expressed in kW/m), while typically 4–6 cracks occur during normal operation in LWR rods [105]. Very little relocation of the fuel pellet "wedges" is noted until the linear rating is in excess of approximately 25 kW/m or the centreline temperature exceeds approximately 1170 °C [104]. Below these thresholds, asperities on the crack surfaces bind the fragments together [98,104]. Above these thresholds, the centre-to-surface temperature gradient drives the crack surfaces apart permitting relative motion of the fuel fragments. An irreversible diameter increase will occur as the fragmented fuel seeks a state of lower free energy [104].

At temperatures where the UO_2 is plastic, cracks in the UO_2 heal quickly [98]. In fact, adjacent pellets, which do not have perfectly matched surfaces, are found to coalesce at temperatures down to 1500 °C [98]. Healed cracks can sometimes be identified as a line of porosity, either spherical or lenticular in shape. Also, the compressive thermal stresses in the fuel centre are reduced due to plastic flow of the UO_2. If a shutdown occurs, a reverse thermal stress field will be created in the once plastic zone causing further radial cracking between the fuel centreline and the edge of the once plastic zone. On a return to power, vapour phase transport of the UO_2 can promote crack filling in this central zone producing a "smooth" central bore at the fuel centreline [98]. Radial cracks do not modify the heat transport within the fuel pellet. In fact, the fuel "wedges" will thermally expand to a greater degree than solid fuel, thereby reducing the fuel-to-sheath gap or increasing interfacial pressure and thus lowering fuel temperatures (see item i in Section 2.1.4).

Circumferential cracks in the central region of the pellet appear on cooling. The crack(s) tends to appear at a pellet radius consistent with the onset of equiaxed grain growth. Fuel grains in this region have a reasonable inventory of grain-boundary porosity and tend to fracture easily. Small-scale circumferential cracking has not been observed to alter the thermal conductivity of UO_2 significantly. Large-scale circumferential cracking represents a "fuel/fuel gap" similar in behaviour to a fuel-to-sheath gap [106,107]. Where a circumferential crack has formed on cooling, hard contact and healing will occur on the following rise to power. Where the circumferential crack is artificially maintained, a temperature drop of less than 60 °C can be associated with such a crack [98]. However, large-scale circumferential cracks do not exist at power in CANDU fuel. Grain-boundary bubbles would be expected to grow by surface diffusion in regions where the "circumferential" cracks in the colder outer rim are associated with the more random fracture pattern caused by thermal stresses. However, since the thermal resistance of these circumferential cracks is quite small

[98], the restructuring patterns seen in the fuel "wedges" align in adjacent fuel pellets due to their inherent temperature sensitivity.

For element linear powers in excess of 25 kW/m, irreversible diameter increases occur as the fragmented fuel seeks a state of lower free energy. The change in fuel pellet diameter due to fragment relocation for unclad pellets, $\Delta D/D$, has been determined and can be described by the expression [104]:

$$\Delta D = c|\Delta q| \tag{7}$$

where ΔD is the change in fuel pellet dimension, c is the relocation coefficient, and Δq is the change in fuel element linear rating above 30 kW/m. At ramp rates exceeding 185 kW/m/h, the relocation coefficient is ~1–2 μm/(kW/m) (and is zero below a linear rating of approximately 30 kW/m). In situations where the fuel fragments are restrained by the sheath, relocation will consume the fuel-to-sheath gap. Fuel relocation is not included in the normal operating CANDU fuel performance codes. Instead, the fuel-to-sheath gap is assumed to be zero for fuel/sheath heat transfer evaluation purposes.

The In-Reactor Diameter Measuring Rig (IRDMR) has been used to determine a direct in-reactor measurement of the fuel relocation. These measurements illustrate pellet expansion due to relocation as well as compliance of the fuel fragments on contact with the sheath at full power [108]. Indirect evidence, from gas release measurements and UO_2 restructuring on fuel fabricated with diametral clearances typical of CANDU fuel, indicate that the fuel and sheath achieve at least light contact during operation (i.e. a minimum fuel-to-sheath heat transfer coefficient of ~7 kW m^{-2} K^{-1}). Good agreement with post-test measurement occurs even when predicted fuel-to-sheath radial gaps of approximately 20 μm exist indicating relocation of at least this amount. CANDU fuel expands about 100 μm due to thermal expansion and cracking in going to high power. The results of in-reactor experiments with fuel elements having thick sheaths and diametral clearances of 100, 200 and 280 μm indicate that light fuel/sheath contact is established for the first two clearances but not for the third [109]. This would indicate an upper limit on fuel diametral relocation of less than 200 μm. Diametral relocation of approximately 30 μm has been measured in the IRDMR tests.

(vii) Molten fuel

UO_2 expands 10.4 volume percent on melting. The expansion improves fuel-to-sheath heat transfer by reducing the fuel-to-sheath gap and/or increasing the fuel-to-sheath interfacial pressure [106,109]. This large differential expansion can be quite noticeable in post-irradiation examination as swelling of the fuel element [110]. UO_2 is a viscous "solid" before melting and a viscous liquid after melting. On cooling, the once molten zone contains gas-filled pores formed by precipitation of gaseous fission products or a gas-filled cavity forms by sublimation of UO_2 and subsequent condensation on cooler surfaces.

When a fuel element defects, the sheath no longer provides a barrier between the fuel and primary coolant. Coolant can therefore contact the fuel, permitting oxidation of both the fuel and inner surface of the sheath. The presence of water vapour in the fuel-to-sheath gap can lead to a degradation in the thermal performance of the fuel element [111]. For instance, the gap heat transfer coefficient will change as steam and hydrogen replace the helium fill gas [111,112]. The fuel oxidation process can lead to a degraded thermal conductivity in the hyperstoichiometric fuel (see item i in Section 2.1.2). In addition, the hyperstoichiometric fuel will have a lower incipient melting temperature (see item iv in Section 2.1.2). Consequently, fuel centreline melting is possible for defective fuel operating at high linear ratings of ~67 kW m^{-1} [113]. A moving boundary Stefan treatment and phase-field model has been developed to describe heat transport and oxygen transport with oxidized fuel which provides a means to track the movement of a phase-change front in the case of fuel centreline melting [114,115].

2.1.4. Zircaloy properties and sheath deformation

Thermophysical properties of Zircaloy can be found in the MATPRO handbooks, including, for example: thermal conductivity, thermal expansion, specific heat and Young's modulus [25].

An accurate model for the deformation behaviour of the Zircaloy sheath is needed to determine the differential thermal expansion of the fuel and the sheath and thus the fuel-to-sheath interfacial pressure. A microstructural sheath creep model is therefore important to assess the fuel temperature during normal and transient conditions. The hoop stress within the sheath that results from the pressure of the fuel pellets and the internal gas pressure causes the sheath material to undergo plastic deformation (or creep), relieving the stress and fuel-to-sheath interfacial pressure. The correlation for the Zircaloy expansion is independent of irradiation history and expresses the axial and radial components of the strain due to thermal expansion as functions of the average sheath temperature. Separate equations are given for alpha-Zircaloy below 1073 K and beta-Zircaloy above 1273 K, with a linear interpolation for the transition region between these temperatures. The thermal expansion in the alpha to beta region accounts for the reduction in volume associated with the phase transition. Data on the thermal expansion of Zircaloy above the beta phase transition temperature of 1073 K are non-existent.

A sheath creep model was initially developed as the separate NIRVANA code for ELOCA, which was independently tested against a large number of sheath strain experiments [116]. This model tracked the microstructural changes in the fuel sheath and included components for: high-temperature annealing (recrystallization), changes in the alpha-phase fraction, and changes in grain size. The high-temperature creep behaviour of the sheath was modelled as three separate components: dislocation creep, grain- or phase-boundary sliding, and strain due to phase transformation. The assumption was made that the ZrO_2 formed on the outside of the sheath did not carry any tensile load, and the thickness of the load carrying portion of the sheath was adjusted to account for oxidation. The model has been modified to account for the strengthening of the sheath caused by the dissolution of oxygen within the sheath and oxidation of the sheath surface (i.e. oxide-strengthening). This model calculates the plastic component of sheath strain as the result of an imposed stress. An important component of this calculation is the determination of the elastic component of the sheath strain. The relationship between the elastic strain and the imposed stress is governed by the Young's modulus of the Zircaloy sheath material (which is a strong function of the sheath temperature). The elastic component of the sheath strain also plays an important role in the determination of the fuel-to-sheath interface pressure.

The NIRVANA model has been validated against 800 out-reactor biaxial and uniaxial sheath strain tests from three independent laboratories. The oxide-strengthening model was also validated against approximately 100 biaxial strain tests conducted in a steam environment at the Chalk River Nuclear Laboratories (CRL). The various criteria identified for sheath failure is detailed in item ii (with a more general overview of power pulse behaviour in Section 2.5).

(i) Fuel-to-sheath heat transfer

Where the fuel and sheath are in good contact either through fuel pellet expansion or creep down of the sheath under coolant pressure, the fuel/sheath heat transfer coefficient will be large and the temperature drop across the fuel-to-sheath gap will be less than ~20 °C.

For operation at element linear powers in excess of 30 kW/m, relocation of fuel fragments will produce a "zero" gap

configuration (as mentioned in item vi of Section 2.1.3). The fuel/sheath contact will probably be light with a fuel/sheath temperature drop of 50–60 °C. For operation below ~30 kW/m, fuel fragment relocation cannot be expected. Both the heat flux across the fuel/sheath gap and the width of the fuel sheath gap are approximately linear functions of the heat rating. The fuel/sheath temperature drop will be nearly constant for these power outputs even in cases where fuel/sheath eccentricity exists [117].

The model used in the ELOCA code to calculate the fuel-to-sheath heat transfer coefficient is a variation of that proposed by Campbell et a1. [118] which, in turn, is based on the earlier work by Ross and Stoute [106]. These models separate the fuel-to-sheath heat transfer coefficient into two separate components: (i) a solid/solid component that accounts for the heat transfer between the solid surfaces of the fuel and sheath when in contact, and (ii) a gas conductance component that accounts for the heat transfer by the gas in the fuel-to-sheath gap. The ELOCA model includes these components, as well as a third term to account for radiative heat transfer that is more important at high-temperature. The ELOCA fuel-to-sheath heat transfer model also accounts for the change in gas composition in the fuel-to-sheath gap with the ingress of steam following a sheath failure.

(ii) Fuel sheath failure criteria

The ELOCA code is used to calculate the timing of sheath failure. A brief description of the sheath failure models and associated failure criteria, as well as the identified data upon which these mechanisms are based, are given below [119,120]. The ELOCA code specifically considers seven mechanisms for determining the possibility of sheath failure:

- *Sheath failure due to overstrain*: Internal gas pressure causes the sheath to strain, balloon, and ultimately burst. A fuel sheath failed in this way generally shows a large degree of sheath strain localized around the failure point. However, the ELOCA code is essentially one-dimensional in nature and is incapable of modelling the large localized deformations that occur just prior to failure. Hence, the failure criterion is based on the onset of plastic instability rather than the sheath strain at failure. The phenomenon of work hardening ensures that the hoop strain of the fuel sheath remains approximately uniform up to some critical point at which a localized instability may occur leading to rapid ballooning to failure. An analysis by Hunt [121] of data collected by Hardy [122] showed that the average sheath strain at the onset of the instability for CANDU sheathing is temperature dependant, but has a minimum value of 5% corresponding to a sheath temperature of 650 °C. This 5% average sheath strain is used as the sheath overstrain failure criterion in ELOCA, however, when interpreting the code results it must be remembered that this criterion represents the potential onset of ballooning rather than sheath failure and is considered to be a very conservative criterion.
- *Low ductility sheath failure*: At temperatures below ~700 K, the sheathing may demonstrate low ductility due to work and irradiation hardening. Under most accident transients, the sheath anneals early in the transient. However, for sudden power increases, the fuel may expand and strain the sheath before annealing can occur and the sheath may fail at low strains of ~0.4%. As mentioned, ELOCA includes a model for the effects of annealing due to recrystallization of α-phase Zircaloy [116]. A failure criterion in ELOCA assumes sheath failure if the "athermal" sheath strain exceeds 0.4% before 95% of the sheath material has re-crystallized. The 0.4% strain value is based on experiments conducted in NRU by Hardy and Bain [123].
- *Sheath failure by beryllium-assisted crack penetration*: Under conditions of high hoop stress and temperature, the presence of beryllium in the region of brazed appendages may initiate cracks and enhance the crack propagation rate by a process termed "liquid metal embrittlement". ELOCA uses a model developed by Kohn and Clendening from measurements of time to failure and crack propagation rates, which is stochastic in nature and provides an estimate of the probability of failure [14].
- *Sheath failure by oxygen embrittlement*: This failure criterion was introduced by Sawatzky where, if the oxygen concentration over half the sheath wall thickness exceeds 0.7 wt.%, the sheath will be sufficiently brittle to fail upon rewet [124]. The criterion is based on measurements conducted by Sawatzky and other researchers. The criterion appears to be well founded and has the advantage of being very similar to a failure criterion used by the US nuclear industry.
- *Sheath failure by overstrain under oxide cracks*: The oxide layer on the surface of the fuel sheath is brittle, i.e., Sagat et al. observed cracks using an SEM at strains as low as 2% (but these cracks are likely to be present at lower strains) [125]. The crack provides a path for oxygen to penetrate into the crack tip. Moreover, a high stress at the oxide tip causes the new oxide to crack further and the crack may propagate into the substrate. The ELOCA code includes a model for crack propagation, where the propagation rate is a function of the hoop stress and the parabolic growth rate of the oxide. The model also includes terms for the localized stress and strain under the oxide cracks. The sheath is deemed to have failed when the localized strain under the oxide crack exceeds a "user-specified" overstrain criteria (i.e. a default value of 15% is used in ELOCA).
- *Sheath failure due to high strain rate*: The sheath is deemed to have failed if the sheath creep rate exceeds 10^{-1} s^{-1}. If the strain rate were to reach this high value then sheath failure is expected very rapidly.
- *Sheath failure due to high fuel enthalpy*: The sheath is deemed to fail if the radially averaged energy deposited in the fuel exceeds 838 kJ/kg UO_2 (however, this failure criterion is no longer used). This criterion is based on power pulse experiments on LWR type fuels and is likely not relevant to CANDU fuel types (see Section 2.5). Fuel centreline melting will occur before this criterion is met.

2.2. Oxidation, hydriding and embrittlement of the Zircaloy sheath

The oxidation of the Zircaloy sheathing is an important consideration in light water/heavy water reactor accidents because this reaction will release heat and produce hydrogen/deuterium gas:

$$\begin{aligned} Zr + 2H_2O &\rightarrow ZrO_2 + 2H_2 \\ Zr + 2D_2O &\rightarrow ZrO_2 + 2D_2 \end{aligned} \quad (8)$$

With a sufficient amount of heavy water vapour, the sheathing can be fully oxidized to ZrO_2 before the melting point of the metal is reached. On the other hand, as a significant amount of deuterium gas can be produced in Eq. (8) with a large mass of zirconium in the fuel channels, the gas phase can become depleted in heavy water vapour in the downstream locations of the fuel channels. In this case, the sheathing does not completely oxidize and the ZrO_2 scale can dissolve into the remaining metal.

In the physical process of sheath oxidation [126], with the absorption of oxygen by the sheathing, the steam mole fraction in the gas at the surface of the sheath is smaller than that in the bulk gas, and the oxygen uptake rate by the solid depends on the water flux through the external gas phase-boundary layer on the sheathing surface such that:

$$D_2O(\text{bulk gas}) \rightarrow D_2O(\text{gas at surface}) \quad (9a)$$

Heavy water decomposition occurs at the solid surface according to the reaction

$$D_2O(\text{gas at surface}) = O(\text{solid at surface}) + D_2(\text{gas at surface}) \quad (9b)$$

The O/Zr ratio in the solid at the surface is related to the heavy water vapour-D_2 ratio in the adjacent gas by the thermochemistry of the O–Zr system. Oxygen in the solid at the surface moves through the oxide scale by solid-state diffusion:

$$O(\text{solid at surface}) \rightarrow O(\text{oxide at interface}) \quad (9c)$$

The oxygen that arrives reacts with the substrate metal to produce the substoichiometric oxide ZrO_{2-x} at the oxide–metal interface

$$Zr + (2-x)O(\text{oxide at interface}) \rightarrow ZrO(2-x) \quad (9d)$$

which equilibrates with the substrate α-Zr:

$$O(\text{oxide at interface}) = O(\text{metal at interface}) \quad (9e)$$

The O/Zr ratio in the metal at the interface is the terminal solubility of oxygen in α-Zr. Oxygen diffuses into the substrate metal from the oxide–metal interface

$$O(\text{metal at interface}) \rightarrow O(\text{bulk metal}) \quad (9f)$$

at a rate determined by the Fick's second law of diffusion.

Large accident modelling codes [127–129] generally describe the Zircaloy oxidation process using parabolic corrosion rate theory developed from laboratory experiments [130–136]. For the parabolic rate law

$$w^2 = k_w t \quad (10)$$

where w is the mass of Zircaloy reacting per unit area with steam (kg m^{-2}), k_w is the reaction rate constant (kg m^{-4} s^{-1}), and t is time (s). The parabolic rate constant k_w, has the form

$$k_w = k_{wo} \exp\left(-\frac{Q}{RT}\right) \quad (11)$$

where k_{wo}, and Q are constants (see Table 1), R is the ideal gas constant (=8.31 J mol^{-1} K^{-1}), and T is the temperature (in K) [137].

Recent experiments at 700–900 °C with steam pressures from 0.1 MPa to 15 MPa suggests that the oxidation rate of Zircaloy-4 increases with the steam pressure; however, this pressure dependence does not appear at 1100 °C [138,139]. Zircaloy oxidation tests were also conducted in various steam–hydrogen mixtures at temperatures between 1223 and 1373 K [140]. In these latter tests the total weight gain varied with the hydrogen volume fraction, and significantly decreased at a critical level of the hydrogen fraction. Hydrogen absorption occurred above a critical hydrogen fraction with the presence of a porous oxide. The hydriding resulted in a reduction in the Zircaloy-4 ductility.

In parabolic corrosion rate theory, the increment in the oxygen absorbed in a time step Δt is taken to be the minimum of $\dot{w}\Delta t$, n_{zr} or $n_w/2$, where $\dot{w}$ is the molar rate of oxygen absorption per square centimeter of sheathing, given by parabolic rate theory, and n_{zr} and n_w are the moles of zirconium and D_2O (or H_2O) per unit sheathing surface area in the node at the start of the time step. These three conditions represent parabolic corrosion in unlimited steam, zirconium availability, and steam availability, respectively. The laboratory corrosion experiments that underlie the above method are isothermal, usually conducted in unlimited steam environments, and are restricted to metal specimens whose thickness is large compared with the scale thickness. Under these conditions, the rates of oxygen uptake and of growth of the oxide scale are theoretically inversely proportional to the square root of time as shown in Eq. (10) [133]. However, in the heavy water vapour-D_2 gas (or steam-H_2 gas) present in a degraded reactor accident, the conditions required for a parabolic behaviour may not be fulfilled. The effect of scale dissolution in the substrate metal, which occurs in steam-starved gases, cannot be modelled by parabolic kinetics. Moreover, this simple approach fails to account for the details of the morphological changes that can occur in steam-starved locations of the fuel channels. The presence or absence of a ZrO_2 scale on the sheathing has a very important effect on the uptake of hydrogen by the metal, which can affect the course of the fuel dissolution process when the metal melts in higher temperature accident scenarios.

Table 1
Parametric values for parabolic rate constant for Zircaloy oxidation in steam[a].

Investigators	Temperature range (K)	k_{wo} (kg^2 m^{-4} s^{-1})	Q ($\times 10^3$ J/mol)
Baker and Just	1273 to melting point	3.33×10^3	190
Urbanic and Heidrick	1323–1853	2.96×10^1	140
	1853 to melting point	8.79×10^1	138
Pawel et al.	1273–1773	2.94×10^2	167
Prater and Courtright	1783–2773	2.68×10^4	220

[a] Taken from Ref. [137].

The oxidized sheathing has a complex morphology. For instance, two other contiguous metallic phases of zirconium can exist for the partially-oxidized Zircaloy sheathing in addition to the zirconia layer. Since the mechanical properties of these layers are strongly influenced by oxygen distribution, an accurate prediction of the layer thicknesses, oxygen profile and reaction rates are needed. Although simple parabolic rate kinetics can be used to estimate layer thicknesses for "thin" layers with a ramp and hold type transient, a diffusion-based calculation is required if the temperature decreases, as well as with the presence of thick layers and non-equilibrium oxygen conditions at the boundary layers. Thus, in summary, a more complicated model is needed to predict the Zircaloy oxidation behaviour to more accurately predict the oxidation kinetics, as well as the sheath deformation behaviour and time of failure. In addition, as mentioned, parabolic kinetics cannot handle the scale dissolution behaviour in reducing environments.

A variety of structures result in oxidized Zircaloy that depends on the temperature and oxygen concentration [141]. At temperatures below 1144 K, an outer layer of zirconia results adjacent to a layer of alpha Zr (α) (which contains oxygen in solid solution). On the other hand, at temperatures above 1255 K, at least three layers are observed: (i) an external zirconia layer, (ii) an intermediate "oxygen-stabilized" α layer, and (iii) an inner layer of base metal comprised of transformed beta Zr (β). Between this temperature range, the transformed β forms at the triple point of the α grains, where three structures form: (i) an outside layer of zirconia, (ii) an α layer adjacent to the zirconia layer, and (iii) an internal layer of transformed β combined with undissolved α. With cooling, the β phase will transform back to the α phase in which the oxygen concentration is significantly different from that of the oxygen-stabilized α and "prior β". Moreover, under certain conditions, the α layer can also consist of two sublayers (α_1 and α_2) [141]. The prior β material can also reveal structural changes where, if enough oxygen is absorbed, "α incursions" may form with a growth of oxygen-enriched α into β. Although the boundaries between the different phases are generally planar, irregular boundary surfaces can be formed at low temperatures or by the appearance of the secondary phenomenon previously mentioned.

As mentioned, diffusion theory has been applied to describe sheathing corrosion for general transient conditions for finite specimens [141–143]. These models are quite accurate but difficult to numerically incorporate into the nodal form of large accident analysis codes because they require the numerical solution of partial

differential equations representing Fickian diffusion in each layer. These partial differential equations are also subject to specified oxygen concentration values at each of the layer boundaries and oxygen conservation relationships as the boundaries move. This moving boundary problem has been solved as the FROM (Full Range Oxidation Model) computer code, which predicts the various corrosion layer thicknesses, transition from two phase to three phase oxidation, and oxygen concentration profiles in the Zircaloy sheath [141]. This latter treatment also incorporates non-equilibrium boundary concentrations that improve the prediction of the oxide layer thickness.

An "integral diffusion technique" has been further developed as a compromise between the computationally simple yet physically oversimplified parabolic kinetic technique and the highly descriptive but analytically complex full diffusion theory treatment [126]. In this method, the exact concentration distribution of oxygen in the metal phase is replaced by an approximate distribution that fits the boundary and initial conditions. This distribution is coupled to the linear oxygen concentration profile in the oxide layer (and ultimately to the steam mole fraction in the bulk gas). However, this treatment oversimplifies the duplex α-Zr and β-Zr metal phase as a single metal layer (with the diffusion properties of α-Zr). Thus, this technique fails to accurately model the structural properties of the sheath, which is particularly important in order to determine the timing of sheath failure. As such, the more accurate FROM code has been numerically implemented into the ELOCA transient analysis code for accurate simulation of high-temperature oxidation of the sheathing. The detailed morphological state of the sheathing is important because it determines: (i) the mechanical properties of the sheath and thus the timing of sheath failure (Section 2.1.4), (ii) the heat released by the oxidation process and hydrogen dissolution in the cladding (Section 2.3), and (iii) the capacity of the metal to dissolve fuel when the cladding melts at ~2000 °C (Section 2.4).

Oxidation of the Zircaloy sheath in air is also important because of the possibility of CANDU fuel handling and end-fitting failure accidents. Single-effects experiments with air-oxidation from ~500 to 1000 °C, as well as multi-element testing in the CODEX facility simulating air ingress for Pressurized Water Reactor (PWR)-type fuel, have been performed [144–147]. In the reaction between Zircaloy-4 and air and in air and nitrogen-containing atmospheres at temperatures above 800 °C, there is a degradation of the cladding material with formation of zirconium nitride and its re-oxidation [148]. Breakaway oxidation in air shows similar characteristics to that of steam, where the only difference is due to the formation of zirconium nitrides. Although parabolic correlations may be applied for oxidation in air, this is only appropriate for high temperatures (>1400 °C) and for pre-oxidized cladding ($\geqslant$1100 °C), i.e., under all other conditions, faster kinetics are observed to occur [148]. Since the FROM code is able to handle breakaway oxidation in steam, it is now being upgraded to simulate air-oxidation phenomenon as well.

Measurements have also been made on the loss of ductility and embrittlement of Zircaloy-4 cladding by oxidation and hydriding under LOCA conditions and with a water quench [149–154]. In particular, the LOFT FP-2 test was a relatively large in-reactor experiment to determine the effect of reflood for a severely damaged core assembly [155,156]. A large fraction of the bundle inventory of the LOFT FP-2 bundle was available for subsequent oxidation during reflooding. This experiment showed that significant H_2 generation can be expected during reflooding, which is largely dependent on the degree of prior oxidation and reflood thermalhydraulic conditions. An upper debris bed was also observed in the LOFT FP-2 test when coolant was introduced into the hot bundle, resulting in a thermal shock and fragmentation of the oxidized fuel rods.

The impact of the oxidation and hydriding process on the chemical heat is detailed in Section 2.3.2.

2.3. Fuel-to-sheath gap processes and heat release

2.3.1. Gap transport

During reactor accident conditions, steam (or heavy water vapour) that enters into a fuel element will interact with the Zircaloy sheath at high-temperature and produce significant quantities of (molecular) hydrogen (or deuterium) gas as a result of the metal–water reaction in Eq. (8). The incoming steam must therefore diffuse against an outgoing current of hydrogen gas produced from the (internal) Zircaloy corrosion reaction as well as from the fuel oxidation reaction itself. In addition, at higher fuel temperatures there is a greater release of fission gas (i.e. xenon and krypton) into the fuel-to-sheath gap from the fuel matrix and therefore a greater outflow current of fission gas. These processes give rise to multi-component transport in the gap, which is particularly important because it can inhibit the internal oxidation of the fuel when the sheath is breached in the early stages of the accident. Any hydrogen production will significantly reduce the oxygen potential in the gap. Thus, in addition to a physical barrier, the sheath also acts as a chemical barrier while oxidation of the sheath is occurring [157–159].

This effect is predicted by previous analysis considering a Stefan–Maxwell treatment for multi-component diffusion in the gap [157] and supported by experimental observations [159]. For example, annealing experiments with mini-length fuel elements at the Chalk River Laboratories show that significant cesium release does not occur until the sheath is completely oxidized [159]. This observation provides indirect evidence that fuel oxidation has not occurred while the sheath is oxidizing as an enhanced fission-product diffusivity will only occur in hyperstoichiometric fuel. Thus, during transient conditions, as a result of significant hydrogen generation by metal–water reaction on the inside surface of the sheath, fuel oxidation is limited until the sheath is practically oxidized. This effect is conservatively neglected in transient fuel analysis with ELOCA.

In summary, steam penetration of the gap is very small, because of the rapid reaction of H_2O with the inner wall of the sheathing. The gap is effectively exposed to pure H_2 at the failure site, even if steam is present in the primary heat transport system (PHTS). The release of inert gases into the fuel-to-sheath gap creates a backflow against which H_2 must diffuse into the interior of the element. In accident scenarios where the fuel element becomes steam-starved, the outer ZrO_2 scale on the sheathing dissolves in the metal. Without a protective oxide scale, hydrogen can permeate through the sheath wall and replace the inert gas in the gap with H_2. The permeated H_2 is recycled to the external gas by flowing out of the sheathing breach. As discussed in Section 2.3.2, adsorption of hydrogen by zirconium is exothermic and the heat released by this process can augment oxidative heating by the metal–water reaction.

2.3.2. Chemical heat

All transient reactor analysis codes including the ELOCA code compute the oxidative heat release from the standard enthalpy change for the reaction in Eq. (8) [127–129]. However, during a substantial portion of the accident, the corrosion-product is not the stoichiometric oxide [157]. As detailed in Section 2.3.1, in the steam-starved regions, the principal final state is oxygen dissolved in the metal so that the heat release is in accordance with the reaction:

$$Zr + H_2O = Zr(O) + H_2 \quad (12)$$

The partial molar enthalpy of solution of oxygen in Zr depends on the O/Zr ratio of the metal, where calorimetric data permit estimation of this quantity [160,161]. For typical oxygen contents in the metal, the heat of solution of oxygen is 3–5% more negative than the heat of formation of stoichiometric ZrO_2. Hence, after subtracting the heat of formation of $H_2O(g)$, the heat release for the reaction in Eq. (12) is 6–10% larger than that for Eq. (8) [157,162].

It is generally assumed that the hydrogen solubility in Zircaloy is negligible at high temperatures. Although the phase diagram of the H–Zr system shows that zirconium hydrides do not form at temperatures above about 1200 K [163], measurements of the high-temperature solubility of hydrogen in Zircaloy, however, show that dissolution as interstitial atoms is significant particularly at a higher system pressure [164]. For high steam flow rates, the outer sheath surface is covered with a protective ZrO_2 scale. Hence, because of the low solubility of hydrogen in ZrO_2 [165], H absorption is restricted to just the pick-up fraction that results during Zircaloy oxidation. This amount is quite small because of the low hydrogen permeability of the coherent oxide scale produced by oxidation above ~1300 K. When a ZrO_2 scale separates the external gas from the metal, the gas in the gap consists of only He and Xe, except for short distances from the rupture site, where some hydrogen and, to a lesser extent, steam are present (see Section 2.3.1). On the other hand, with a low steam flow rate, the external gas quickly becomes steam-starved and, shortly thereafter, the oxide scale dissolves into the metal (Section 2.2). Regions of the channel that contain Zircaloy without an oxide scale are inevitably in contact with a gas that is nearly pure H_2, which dissolves in the metal according to the reaction:

$$H_2(g) = 2H(abs)$$

The equilibrium of this reaction is given by Sievert's law:

$$\frac{C_H}{\sqrt{p_{H_2}}} = \exp\left(\frac{\Delta S_H}{R}\right)\exp\left(-\frac{\Delta H_H}{RT}\right) \tag{13}$$

where C_H is the H/Zr ratio of the metal in equilibrium with the gas containing H_2 at a hydrogen gas partial pressure p_{H_2} (atm). The thermochemical properties of hydrogen dissolution in Zircaloy are given in Table 2 [164,166,167]. However, some discrepancy is seen in the measured values shown in Table 2. Hydrogen dissolution is typically neglected in current accident analysis even though the above data suggest that the solubility is significant at temperatures as high as 2000 °C. The principal consequences of hydrogen retention by the metal are twofold [157,162]: (i) the unoxidized metal acts as a sink of hydrogen, which can alter the timing of hydrogen release; hydrogen absorbed in the metal in the steam-starved regions of the channel is released on subsequent oxidation, because of the low solubility of hydrogen in zirconia. (ii) Hydrogen absorption by zirconium releases heat.

The normal approach for estimating heat release as considered in accident codes is by oxidative heating which is valid during the early stages of a transient because the principal oxidation product is ZrO_2, and the oxide scale has not appreciably dissolved in the metal so that no hydrogen is absorbed in this time period. This oxidative heating is based on the total amount of oxygen absorbed, assuming that the heat released per gram atom of oxygen absorbed by the metal is one-half of the standard enthalpy of the reaction in Eq. (8). As previously discussed, in steam-starved regions, one must further consider the effect of oxygen absorption in metallic Zr. Moreover, hydrogen absorption can result in a sharp increase in the heat release with dissolution of only 10% of the corrosion-product hydrogen in sheathing without an oxide scale, i.e., while not as exothermic as oxidative heating, hydrogen uptake can nearly double the contribution from oxidation alone [157]. This additional heating effect is the sum of the product of the hydrogen content of the metal and the enthalpy of solution of hydrogen. The cumulative heat release will decrease with a reduction in the solubility of hydrogen in Zr as the temperature increases [157]. Desorption of hydrogen from the cladding is endothermic, which consumes more heat than is typically provided by the continuing oxidation process.

Table 2
Thermophysical properties for hydrogen dissolution in Zircaloy.

Investigator	ΔH_H (kJ/mol)	ΔS_H (J/mol K)	Ref.
Moalem and Olander	−63	−54	164
Yamanaka et al.	−246 (alpha), −252 (beta)	−38 (alpha), −25 (beta)	166
Steinbruck	−65	−101	167

2.4. Zircaloy/uranium dioxide interaction and fuel dissolution by molten cladding

Under high-temperature conditions, a combined external and internal oxidation of the fuel sheathing can occur due to a reaction of steam on the outside surface of the sheath (Section 2.2) and from the UO_2 on the inside surface. The UO_2 and Zr can interact chemically at temperatures as low as 1273 K, leading to a complex series of reaction layers [168] where, from both internal and external oxidation, the following reaction layers can be formed [143]: $[UO_2 + U] \rightarrow [\alpha\text{-}Zr(O)_a + (U, Zr)] \rightarrow (U, Zr)$alloy $\rightarrow \alpha\text{-}Zr(O)_b \rightarrow \beta\text{-}Zry \rightarrow \alpha\text{-}Zr(O)_c \rightarrow ZrO_2$. This internal interaction requires a substantial external overpressure to promote good solid–solid contact between the fuel and sheath. The experiments of the KfK group utilized an overpressure of 4 MPa [168], and the AECL experiments were conducted at an overpressure of 1 MPa [169]. In the CANDU fuel design, the thin sheath will creep down onto the fuel under the conditions of the high pressure coolant. However, contact between the sheath and fuel can be lost during the transient with sheath lift off due to fission gas release into the (small) free void space of the fuel element and depressurization with coolant blowdown, as well as with the eventual bursting of the sheath. Thus, with an open gap during an accident, any direct fuel/sheath interaction is suppressed and no uranium is transferred from the fuel to the sheathing as long as the sheath is solid. However, if the gap contains hydrogen, fuel reduction can occur as oxygen moves from the fuel to the sheathing by the H_2O–H_2 transport mechanism, driven by the difference in the oxygen potential between the fuel surface and the sheathing inner wall. However, the extent of fuel reduction and cladding oxidation by this mechanism is minor [157].

ELOCA-IST 1.0 has been further coupled to the sheath oxidation model FROM_SFD (Full Range Sheath Oxidation Model_Severe Fuel Damage), i.e., FROM_SFD is not only capable of modelling the Zircaloy oxidation on the outside of the sheath; it is also capable of simulating the Zircaloy/UO_2 interaction on the inside of the sheath [15]. A moving boundary finite-element scheme is used to solve the oxygen diffusion equations in each region and calculate the oxygen concentration as a function of position within the sheath. However, in this initial implementation, only the information on the outside sheath oxidation is used by ELOCA (i.e. information on the UO_2-Zircaloy interaction is calculated by FROM_SFD but it is not passed to ELOCA) [15].

At temperatures above ~1470 K, steam oxidation of Zircaloy and stainless steel produces a significant temperature escalation. With the melting of the as received metallic Zircaloy-4 cladding (2030 K) or metallic oxygen-stabilized α-Zr(O) phase (2245 K), the solid UO_2 may be partially dissolved and liquefied ~1000 K be-

low its melting temperature. The driving force for the reaction is diffusion of oxygen from the UO_2 into the sheathing. This process has been extensively studied in single-effect laboratory crucible experiments, and models of the kinetics of the phenomenon have been proposed [168,170–186].

In hydrogen-rich regions of the core, the outer oxide scale is not present on the cladding, which is all-metal with oxygen in solid solution. On melting of the cladding, the liquid metal contacts the solid fuel and dissolution of the fuel begins. The endothermic reaction of UO_2 dissolution in U–Zr–O melts and the melting of α-Zr(O) sheathing is affected by the supply of heat. In addition to receiving additional oxygen, uranium from the fuel dissolves in the liquid metal forming a U–Zr–O melt. Dissolution continues until the melt is saturated in both oxygen and uranium [162]. The fuel dissolution process has been detailed, for example, in Ref. [180], where it is shown that diffusion in the growing U–Zr–O melt is rapid and the liquid phase concentration remains at saturation. Reduction of the fuel by oxygen diffusion affects the amount of oxygen in the melt. The effect of an oxide scale will also reduce the extent of fuel liquefaction because less metal is available to dissolve uranium when a melt forms. In addition, the high concentration of oxygen in the oxide layer will increase the oxygen content of the melt, thus depressing the uranium solubility. It is suggested that the fraction of the fuel pellet that is dissolved by the initial liquefaction is small [180].

Experiments specific to the Pickering CANDU fuel design have been performed at ~2000 °C in both an inert and steam atmosphere in a horizontal geometry using annular fuel pellets encased in a Zircaloy-4 cladding with an internal tungsten heater [170]. The extent of the interaction in these experiments depended on the degree of wetting of the UO_2 by the molten Zircaloy-4, i.e., the wetting depends on the oxygen content of the Zircaloy-4 where pure Zircaloy-4 wets UO_2 poorly compared to that of oxygen-saturated α-Zr(O). As expected, the cladding melted over a range of temperature from 1760 °C up to the melting point of the oxygen-stabilized α-Zr(O) at 1970 °C. The tests were held for 1 s to 10 min on reaching 2000 °C. All of the cladding (except ZrO_2 which has a melting point of 2665 °C) melted to form a homogeneous (Zr, U, O)-alloy phase. This alloy phase reacted with solid UO_2 to pick-up more uranium and oxygen. The UO_2 is consequently reduced to UO_{2-x}. When the UO_{2-x} is further depleted in oxygen, the UO_{2-x}/U solvus boundary of the U–O phase diagram is reached. At this point, liquid uranium forms in the UO_{2-x}. On cooling to room temperature, the UO_{2-x} plus liquid uranium forms stoichiometric UO_2 and α-U along UO_2 grain boundaries and in the UO_2 grains. The amount of UO_2 dissolved by the cladding is a function of the cladding volume relative to the UO_2 volume. Only ~0.5–6 vol.% were dissolved in the inert tests in the (Zr, U, O)-alloy phase and even less UO_2 was dissolved in the steam tests due to a reduced driving force for UO_2 dissolution.

The effects of fuel collapse, UO_2/Zircaloy interaction and fuel dissolution have been studied with irradiated fuel samples in several high-temperature tests conducted out-reactor with PWR, Boiling Water Reactor (BWR) and MOX fuel samples [186–191]. For instance, in experiments at the Institute for Transuranium Elements in Karlsruhe using both fresh and irradiated clad samples of UO_2 and MOX at temperatures between 1700 and 2200 °C, the irradiated samples dissolved to a greater extent compared to the fresh samples in the Zircaloy and dissociated into fragments during dissolution [186].

Possible fuel swelling with UO_2/Zircaloy interaction depends on the fuel burnup, peak temperature, time at temperature, extent of UO_2/Zircaloy interaction and amount of gas in the grain-boundary bubbles at the start of the transient. For instance, porosity of ~30% has been observed in high-burnup LWR fuel (53 MWd/kgU) for test temperatures of 2270 K in the presence of molten Zircaloy [185,186]. In the only in-reactor CANDU fuel test (BTF-107) to measure fuel swelling under such conditions, only modest swelling with a 10% increase in diameter occurred for the previously irradiated fuel element (6 MWd/kgU).

2.5. Fuel behaviour during a power pulse and fuel fragmentation

(i) Power pulse tests

A Reactivity Initiated Accident (RIA) in a CANDU reactor during a large break Loss of Coolant Accident (LOCA) would subject the fuel to a longer duration, lower amplitude power excursion than that in a LWR. In particular, RIAs are characterized by power pulses that occur over ~100 ms in LWRs compared to about 1 s in a CANDU reactor. As such, the peak fuel element powers in LWR RIAs typically range from 7 to 12 times the full power rating from starting power levels of 1% full power (or lower) compared to 6 to 9 times full power for a CANDU LOCA starting from 100% full power.

The energy generated in the fuel during the power pulse is a key parameter that governs the fuel response. As summarized in Table 3 [192,193], RIA tests have been performed on different types of fuel in various research reactors over the past three decades that include [194–216]: (i) LWR fuel (i.e. programs in the Special Power Excursion Reactor Test (SPERT) in the Capsule Driver Core (CDC) facility, Power Burst Facility (PBF), Nuclear Safety Research Reactor (NSRR), and French CABRI reactor, (ii) VVER fuel (i.e. tests in the Impulse Graphite Reactor (IGR)), and CANDU-type fuels (i.e. tests in the PBF facility and TRIGA-ACPR (Annular Core Pulse Reactor)). The fuel failure modes that have been identified in these tests include (see also item ii in Section 2.1.4) [193]:

- Oxygen embrittlement (OE) of fuel sheaths due to the Zircaloy–steam oxidation reaction followed by clad cracking on subsequent thermal quench of the test rod. This failure mode occurs well after the power pulse.
- Pellet clad mechanical interaction (PCMI), which typically occurs during, or shortly after the power pulse, with the fuel sheath still relatively cool. The failure is associated with high strain rate loading of the sheath due to rapid thermal expansion of the pellet. Failures can occur at relatively low-energy deposition levels if the clad has lost ductility due to hydriding, development of thick oxide layers and spalling of the oxide.
- High-temperature burst (HTB) (creep strain failure) resulting in a local bulge and split in the sheath. A fuel sheath temperature in excess of the alpha–beta-Zircaloy transition temperature and an internal fission gas pressure higher than the external coolant pressure are pre-requisites for this type of failure.
- Fuel fragmentation (FR) can occur at high fuel enthalpy and involves extensive fuel melting and internal pressurization of the rod prior to clad failure. Significant amounts of molten fuel can be relocated out of the failed rod. Evidence of prior melting is apparent from the spherical shape of the solidified fuel "particles" collected after an experiment.
- Fuel dispersal (DIS), which may correspond to fuel fragmentation for fuel with burnup less than approximately 42 GWd/tU, but which is a significantly different process for high-burnup LWR fuel. It has been suggested that expanding fission gas (i.e. in the grain boundaries as intergranular bubbles) can provide the energy to move solid fuel particles [217]. At high burnups greater than ~40 GWd/tU, a "rim" region will gradually develop at the outer periphery of the fuel of approximately 100 μm in depth [218]. This region is characterized by defect clusters of extremely tangled dislocations, loss of as-fabricated grain-boundary, fine re-crystallized grains of 50–200 nm size and

Table 3
Summary of RIA experiments.

Test reactor	Fuel type	Enrichment (%)	No. test rods	Pellet OD (mm)	Clad material	Clad diam. (mm)	Clad thickness (mm)	Internal pressure (MPa)	Pulse height width (ms)	Failure mode[b]	Lower bound enthalpy (cal/g)	Ref.
SPERT-CDC	BWR	7.0	22	10.6	Zr-4	12.52	0.86	0.1	4	PCMI	154	194
								0.1		CMELT	206	
								0.1		FR	275	
SPERT-CDC	BWR	10.5	5	10.6	Zr-4	12.52	0.86	0.1	4	PCMI	226	194
								0.1		CMELT	274	
								0.1		FR	292	
PBF	PWR	5.8	5	9.29	Zr-4	10.72	0.62	0.1	4	PCMI	185	194
								0.1		FR	350	
NSRR	PWR	10.0	>1200	9.29	Zr-4	10.72	Multiple	0.1	3–4	OE	199	195–207
							0.57–0.9	0.1		PCMI	164	
								1.2		HTB	195	
								2		HTB	162	
								3		HTB	135	
								5		FR	220	
IGR	VVER	4.4	23 Watercooled	7.48	Zr-1% Nb	9.1	0.63	1.7-2	630–840	HTB	141	208–210
			23 Aircooled					1.7-2		HTB	102	
								1.7-2		FR	284	
CABRI	PWR	High-burnup	10	8.2	Zr-4	9.5	0.64	0.4	9–75	DIS	30	211–213
										PCMI	82	
TRIGA-ACPR	CANDU	10.0	12	12.15	Zr-4	13.08	0.4	0.1–2.2	[a]	OE	170	214, 215
										HTB	136	
PBF LOCA	CANDU	10.0	4	12.15	Zr-4	13.08	0.4	0.4–1.09	4–6	OE		216

[a] 53–100 kW/m in 1 s.
[b] See text for failure mode abbreviation.

coarsened pores surrounded by re-crystallized grains. Following sheath failure, the fuel in the rim region can be ejected and dispersed as fine fuel particles that do not present the recognizable spherical shape of prior melted fuel particles. This failure mode is not applicable to CANDU fuel since the burnup is too low to give rise to a rim region.
- Clad melting (CMELT) occurs for a Zircaloy sheath at a temperature of 1860 °C. The energy deposition values for clad melting are similar to those associated with oxygen embrittlement failure and the two mechanisms frequently occur together.

An analytical treatment has been further developed to characterize CANDU-type fuel behaviour under power pulse conditions based on the experimental data, in which the following conclusions can be drawn [193]:

- Threshold values of fuel enthalpy for clad melting and fuel fragmentation failures are not strongly dependent upon the power pulse width and increase slightly with the pulse width due to an increased heat removal by the coolant. Clad melt failure occurs at similar, but slightly higher enthalpy values than that for oxygen embrittlement.
- Threshold values of fuel enthalpy for oxygen embrittlement failure tend to increase with increasing pulse width due to the larger sensitivity of fuel sheath temperature to energy removed by the coolant. The fuel sheath failure mode changes from oxygen embrittlement failure (during a thermal quench) to high-temperature burst as the pressure difference between the inside of the fuel element and the outside coolant increases.
- PCMI failure has a strong sensitivity to pulse width. The threshold fuel enthalpy for failure increases rapidly with increasing half height pulse width. Additionally, for this mode of failure, very small gaps between the fuel pellet and sheath is necessary. It is for this reason that PCMI failures have been observed in RIA tests with short pulse widths (4 ms) and irradiated fuel, while unirradiated fuel tends not to exhibit this failure mode. PCMI is an unlikely failure mode for CANDU fuel because of the long power pulse.
- Fuel fragmentation for fresh and irradiated rods with fuel sheaths that maintained ductility (i.e. sheaths without the excessive corrosion observed on LWR high-burnup fuel cladding) is associated with gross melting of the fuel (see item ii below).

(ii) Fuel fragmentation

Evidence from the RIA tests on fresh and irradiated fuel with burnup less than 40 Gwd/tU show that fragmentation of the fuel is associated with ejection of molten material from the fuel. The maximum fuel temperature for power pulses from cold zero power initial conditions occurs at the surface of the fuel pellet. The enthalpy at the surface of the pellet as a function of the radial average energy deposition is shown in Fig. 1 for various fissile enrichments [193]. Also shown is the enthalpy for liquid UO_2 formation, which is the sum of the enthalpy for onset of melting in the solidus phase plus the heat of fusion (259 kJ/kg). The range of energy deposition for fuel fragmentation from RIA tests is also shown in Fig. 1. This clearly indicates that fragmentation of fuel with ductile cladding is associated with melting at the periphery of the fuel pellet and is strongly influenced by the radial fission power distribution (governed by the fissile enrichment).

2.6. Severe fuel deformation behaviour

The important melting and chemical interaction temperatures, which result in the formation of liquid phases with temperature escalation in PWRs, are shown in Fig. 2. Depending on the accident sequence, in accordance with Fig. 2, the important physiochemical material behaviour include [219,220]:

(i) melting of the Ag–In–Cd absorber alloy at ~1073 K (and, on melting of the stainless steel alloy cladding of the control rod at 1720 K, chemical interactions with the Zircaloy guide tube and fuel rod cladding),
(ii) plastic deformation and bursting of the cladding at ~1020–1370 K (depending on the system pressure),

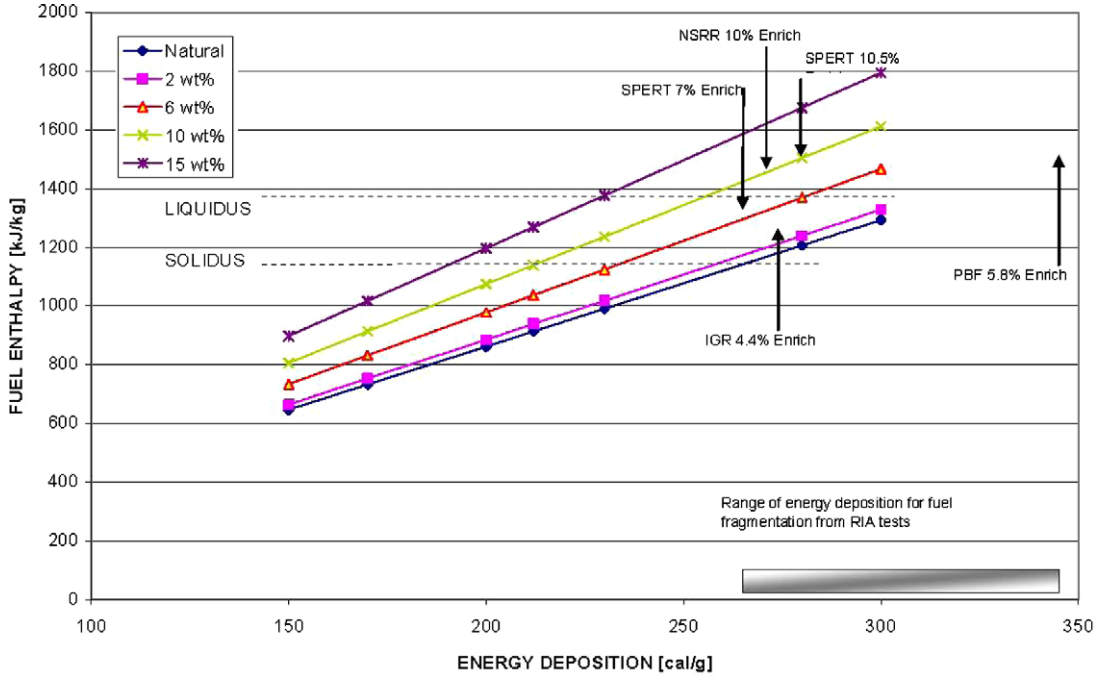

Fig. 1. Fuel enthalpy at pellet surface as a function of energy deposition (fresh fuel, zero power cold pulse) [193].

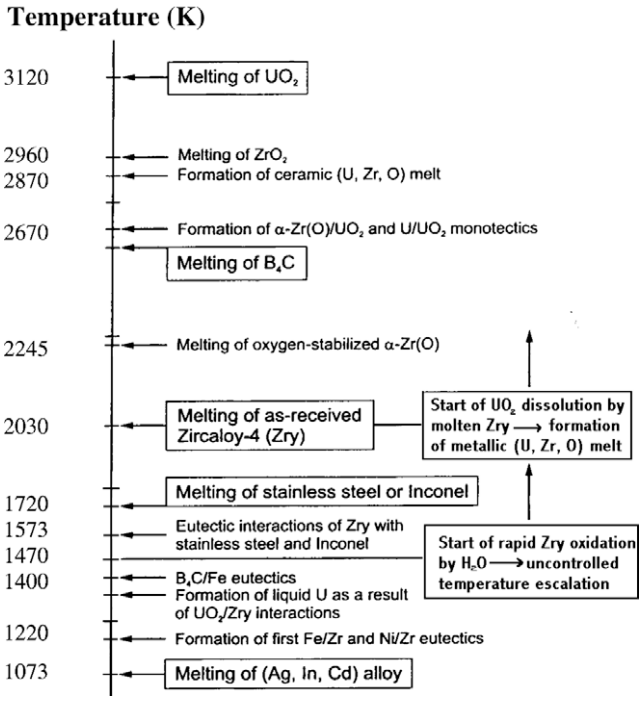

Fig. 2. Chemical interaction temperatures.

(iii) steam oxidation of structural materials (e.g. stainless steel and Inconel) and fuel rod materials (e.g. Zircaloy and UO_2) at ~1470 K, leading to a rapid temperature escalation and the possibility for fuel rod fragmentation,

(iv) eutectic interactions of Zircaloy with stainless steel (e.g. control rod cladding) and/or Inconel (e.g. grid spacers) at 1573 K, interaction of Zircaloy with UO_2 (with hard solid contact) initially below ~1770 K, and melting of stainless steel or Inconel by ~1720 K,

(v) melting of the as received metallic Zircaloy-4 cladding (2030 K) or the metallic oxygen-stabilized α-Zr(O) phase (2245 K),

(vi) reduction of the UO_2 fuel due to interactions with solid and/or molten metallic Zircaloy (i.e. starting at 2030 K), resulting in a partial dissolution of UO_2 with the formation of a metallic Zr–U–O melt (containing ceramic (U, Zr)O_{2-x} precipitations at higher oxygen concentrations),

(vii) relocation of the liquid and solid materials with formation of immiscible metallic and ceramic melts in different parts of the reactor core (>2030 K),

(viii) melting of the ZrO_2 (2960 K) and UO_2 (3120 K) forming a ceramic melt.

Numerous in-pile [221–240] and out-of-pile experiments [241–246] have been conducted to better understand the progression of severe accidents in LWRs as detailed in Ref. [16]. These experiments have principally focused on high-temperature core melt progression and fission-product release behaviour. Specifically, experiments have been designed to investigate: (i) how the core loses its original geometry as a result of interactions between core materials and fuel liquefaction, (ii) the relocation behaviour of the core with melt formation leading to partial core blockage, fuel debris beds and molten pools, (iii) how much hydrogen is produced by the steam oxidation of core materials with relocation, (iv) the influence of core degradation on the release, transport and deposition of fission products and aerosols, and (v) the fragmentation of the degraded core with cool down and/or quenching [247–252,220].

2.6.1. CANDU fuel element/bundle deformation behaviour

Experimental programs have been specifically performed to provide an understanding of the deformation behaviour of CANDU fuel during a LOCA [253]. A model has been developed and verified against in-reactor data to describe the bending of a fuel element (i.e. element bowing) under normal operating conditions that can result from thermally-induced, hydraulic drag and mechanical-load bending moments [254]. This model has been extended to

deal with fuel element bow under post-dryout conditions [255] and tested against the observed fuel behaviour in the U-111 fuel dryout experiment [256].

At more severe conditions with the occurrence of molten material, the relocation of such material in CANDU fuel is expected to be different than that in LWR fuel because of the horizontal geometry of the CANDU fuel bundles. In particular, solid/liquid interfacial forces tend to dominate the relocation of molten materials in thin-walled horizontal CANDU fuel compared to gravity in LWR fuel. CANDU tests with a single, horizontal fuel-element-simulator (FES) where initially performed. Only in excess of 10 °C/s was (minor) circumferential movement of the melt observed. In high-temperature trefoil experiments conducted in an inert atmosphere, local inter-element relocation was observed in the interior triangle subchannel, where the molten Zircaloy relocated into the vicinity of the contact lines between the horizontal elements. Similar inter-element relocation patterns were also observed in high-temperature bundle sag (HTBS) experiments where full-scale fuel bundles were heated by a superheated hydrogen torch. A summary of the phenomena that occur in these high-temperature out-reactor CANDU fuel tests are given below.

At higher temperatures, fuel elements can also bend or sink downward (i.e. sag) from their weight or pressure. Out-reactor tests at Westinghouse Canada Limited (WECAN) were performed in an inert environment on indirect electrically-heated fuel elements (28-element design) to study the sag behaviour at temperatures less than 1200 °C. The SAGC computer code has been used to predict the sag behaviour in these out-reactor tests. Additional laboratory experiments have been undertaken at the Whiteshell Nuclear Research Establishment (WNRE) to study the sag of individual elements in both an inert and oxidizing environment over the temperature range of 1000–1800 °C. Laboratory experiments at WNRE were performed on both Bruce- and Pickering-type endplates to study their deformation behaviour at 1400, 1600 and 1800 °C in an inert environment.

Single-element, out-reactor tests have been performed at the Canadian General Electric (CGE) and WECAN using indirect, electrically-heated, fuel elements to study the deformation behaviour in an inert environment at temperatures below 1100 °C, and at the WECAN for a study in oxidizing environments. As mentioned, WNRE tests also used electric-heated FESs in inert and oxidizing environments to study fuel element deterioration when the sheath temperature exceeded 1850 °C. Other tests have been performed in a pure hydrogen environment in which brittle failure of the sheath was observed. More complex out-reactor tests with seven-element clusters with indirect electrically-heated fuel elements were carried out at the CGE and WECAN to investigate fuel deformation in inert and oxidizing environments below 1100 °C. All effects tests on prototype CANDU fuel bundles in a horizontal orientation were further investigated in several experiments. For instance, furnace-heating tests have been carried out on unirradiated and unpressurized fuel bundles with full-length Pickering bundles and three-quarter length Bruce fuel bundles. A full-length, unirradiated, unpressurized Bruce fuel bundle was also heated by direct resistance to elevated temperatures until the bundle collapsed onto a pressure tube segment. In addition, as mentioned, a hydrogen torch was used to heat a fresh, full-length Bruce bundle to sheath temperatures in excess of 2000 °C in the HTBS program [257,258]. Although molten material formed in these latter tests and relocated to inter-pellet gaps, cracks in the fuel pellets and regions of inter-element contact (i.e. dissolution of the sheath oxide further occurred at these contact points), all tests indicated that the bundle geometry was maintained (Fig. 3) [258]. Other horizontal-oriented bundle experiments have been performed using fuel-element-simulators in multi-element tests with non-prototypic materials [259,260].

Tests on fuel samples from intact and defected fuel elements previously irradiated at 57 and 28 kW/m to burnups of 193 MWh/kgU and to 88 MWh/kgU, respectively, were power ramped using a direct-electric-heating (DEH) method in the Power Pulse 1 experiment at the Chalk River Laboratories (CRL) [261]. These out-reactor tests were designed to investigate fuel behaviour and fission-product release from irradiated fuel for conditions above the upper limit of a LOCA power pulse in which fuel melting occurs. Here samples were typically held for 10 s at a preconditioning power of 12 kW/m, slowly ramped to a steady-state power level of 20 kW/m (and held at this power for 60 s), then quickly ramped to between 30 and 50 kW/m over 5 s, and held at this power for 10 s before termination of the test. Although most of

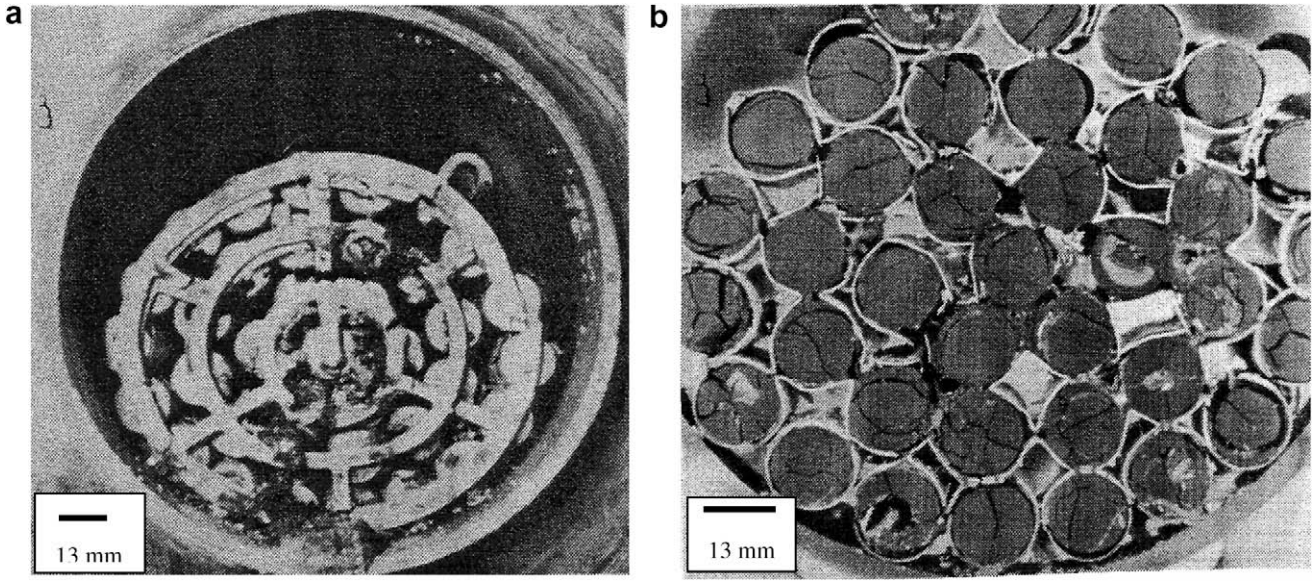

Fig. 3. Cross section of the bundle subjected to a high-temperature plasma torch. (a) View of upstream end of the bundle. (b) View from 30 mm from the front endplate. Note the oxidation of the fuel sheaths, presence of molten material in the subchannels and element contact points. Taken from Ref. [258].

the samples experienced centreline melting, no phenomena were detected that indicated extensive fuel breakup or release of noble gases greater than the grain-boundary inventory fraction.

Based on these various out-reactor experiments, the following understanding of high-temperature fuel behaviour has been obtained [262]. The relatively larger masses of Zircaloy in LWR fuel produce a much larger inventory of melt available for relocation than is possible with CANDU cladding. Since the thin-walled cladding is distributed horizontally, there is not enough Zircaloy mass to accumulate so that liquid/solid interfacial forces (i.e. as opposed to gravity) dominate the relocation patterns. Movement of melt is determined by the adhesive/cohesive properties of the melt, i.e., if the adhesion forces are greater than cohesion forces, the melt will spread (i.e. or "wet") the adjacent solid surface, otherwise the melt will tend to run. The wetting properties of molten Zircaloy depend on the dissolved oxygen content (requiring an oxygen concentration of at least ~1 weight percent). As mentioned in Section 2.4, Zircaloy wets ceramic UO_2 very poorly (with a wetting angle of $\theta \sim 130°$), while oxygen-saturated Zr(O) wets significantly better ($\theta \sim 20°$). The FES tests demonstrated that: (i) inter-element relocation requires a rapid heatup rate of 10 °C/s to the Zircaloy melting temperature (or slower transients with steam starvation), and (ii) that the elements are in contact with each other. The latter condition requires a ballooned pressure tube, where a bundle will settle and elements distort at cladding temperatures typically ranging from 1200 to 1400 °C. Initial contact early in the transient acts to widen the temperature and oxygen profile non-uniformities around the element circumference (Fig. 4). In the contact area, the sheath oxide layer stops growing due to localized steam starvation. Convective heat removal is impaired in this region. The ZrO_2 thickness will become even thinner as the heatup progresses as the underlying metal depletes the oxygen content (Section 2.2). Following melting of the metal substrate, the ZrO_2 shell will be perforated at its thinnest cross section with stress and dissolution of the shell (Fig. 4). Capillary forces are also capable of moving the molten material into inter-element spaces. However, the surface area of the relocated melt will be smaller than that of the original uniformly-distributed cladding; in fact, the reduction in Zircaloy surface area will limit the subsequent exothermic oxidation. Capillary flow of molten material into the UO_2 fuel matrix will also occur, which depends on the oxygen content of the melt to sufficiently wet the ceramic as well as the availability of capillary volumes.

In-reactor tests of four elements of a CANDU 37-element design were tested in the Power Burst Facility (PBF) at the Idaho National Engineering Laboratory [263]. These tests were characteristic of a (power pulse) LOCA transient in the CANDU reactor (Section 2.5), i.e., full power initial conditions with a large coolant depressurization rate and simultaneous power increase before a decrease to decay heat values, where sheath temperatures reached 1000 °C. Failure was observed in one element (small pin hole) at a high sheath strain of ~26% while two of the four elements remained intact [263]. In addition, in-reactor tests of CANDU fuel under accident conditions were also performed in the Blowdown Test Facility (BTF) program [264]. In the BTF-107 experiment a three-element cluster of CANDU-sized fuel elements was subjected to severely degraded cooling conditions resulting in a high-temperature ($\geqslant$2770 K) transient [265,266]. A flow blockage developed during the test due to relocation of U–Zr–O alloy and the high-temperature transient was terminated with a cold water quench. The other three experiments in the BTF program, BTF-104, BTF-105A and BTF-105B, were conducted with single CANDU-sized fuel elements at maximum temperatures of 1800–2200 K in a steam-rich environment (~5 g/s steam supply flow). The BTF-104 experiment pro-

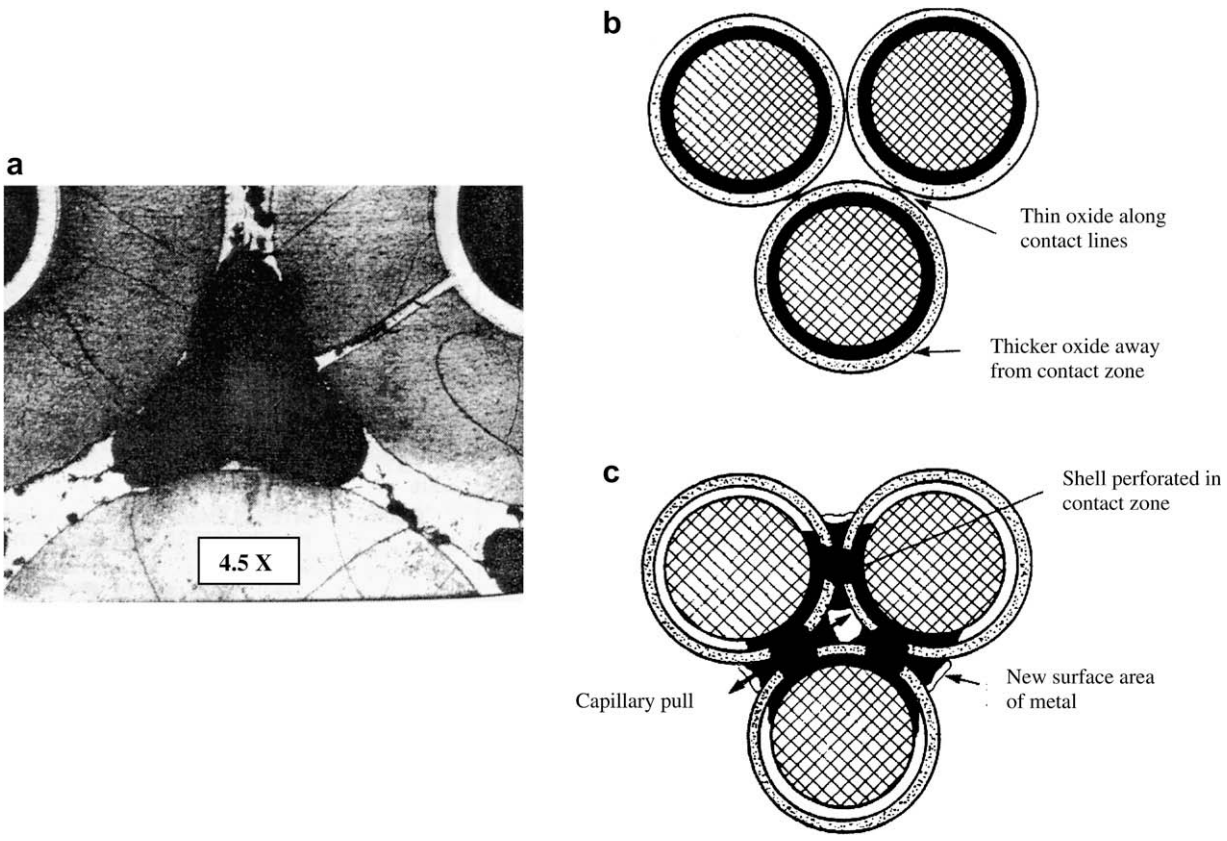

Fig. 4. (a) Local relocation patterns in multi-element horizontal geometry. Schematic of melt relocation phenomena: (b) with onset of melting and (c) after relocation. Taken from Ref. [262].

vided data on fuel behaviour, and volatile fission-product release and transport from a previously irradiated fuel element at a fuel temperature of about 1800 K [267–269]. The primary objectives of the BTF-105A experiment performed were to obtain data for validation of transient fuel performance codes and to test instrumentation for the BTF-105B experiment [270,271]. The BTF-105B experiment had thermalhydraulic boundary conditions which were better quantified and was performed to investigate fission-product release and transport from a previously irradiated fuel element at a fuel temperature of 2100 K [272,273]. Data from BTF-107, BTF-104 and BTF-105A experiments were used to qualify the transient fuel code ELOCA [14], while data from BTF-105A experiment were used to validate the fuel and fuel channel safety analysis code FACTAR [274]. The fission-product release, deposition and aerosol measurements from the BTF-104 and BTF-105B tests are also being used to validate the fission-product release code SOURCE and the fission-product transport code SOPHAEROS [275,276].

2.6.2. CANDU fuel high-temperature annealing tests

More than 300 annealing tests of fission-product release from clad and unclad irradiated fuel samples have been conducted by AECL at temperatures from 800 to 2350 K in Ar/H_2, steam and air atmospheres [277–282]. This work shows that releases of volatile fission products (Kr, Xe, I, Cs and Te) are relatively low in inert or reducing atmospheres but increase significantly after clad oxidation in oxidizing atmospheres. In some of the high-temperature tests on unclad fuel samples, large fractions of the UO_2 fuel was volatilized, leading to releases of fission products that are normally soluble in the UO_2 by the "matrix stripping" process [277,278]. The release rates of volatile fission products from clad fuel samples after complete clad oxidation are almost independent of temperature in the range 1670–2140 K [282]. The low-volatile fission products released in hydrogen-rich atmospheres (Eu, Ba, etc.) are different from those released in steam (Mo, Ru, Nb, etc.) due to chemical effects on the fission-product volatility.

2.6.3. Future directions

To account for fuel bowing phenomena, which can arise for instance with local sheath dryout, the the BOW code has been developed to predict fuel bundle deformation behaviour by considering the fuel elements as composite beams consisting of the sheath and pellets [283]. To model the gripping interaction between the fuel pellets and sheath, empirical factors (i.e. the "Curvature Transfer Factor" and the "Rigidity Enhancement Factor") have been employed. However, physically-based, surface-contact models may be warranted to model the pellet/sheath contact in order to account more fundamentally for the fuel element rigidity. The end plates of the bundle have also been modelled more recently using beam finite elements, which replaces earlier work with the end plates modelled as equivalent torsional springs [284]. A complete bundle deformation model is particularly needed to assess aging effects and the impact of channel sagging on bundle geometry and subchannel thermalhydraulics. This latter phenomenon can lead to the possibility of coolant bypass over the bundle in the horizontal channel design of the CANDU reactor. The BOW code is only applicable to normal operation. However, a capability for transient and more severe reactor accident conditions is needed. For instance, at higher temperatures up to and above ~1000 °C, models are needed to account for bundle sagging and eventual bundle slumping with the loss of endplate integrity to assess the coolability of the bundle for safety analysis.

As detailed in Section 2.6.1, a number of out- and in-reactor tests have been performed to study sheath dryout and fuel element/bundle deformation phenomena. For instance, in-reactor tests were performed in the: organic cooled WR-1 reactor and various loop tests in the NRX and NRU reactor at the CRL. A number of out-reactor tests were also performed to identify single-effects phenomena, including: pickering-design fuel element sag tests at WNRE; sheath sag tests at WECAN; and CRL fuel pin rigidity tests. Out-reactor testswere also carried out to study integrated effects, including: HTBS experiments; CGE inert bundle sag tests; WNRE fuel bundle sag and slumping tests with electrically-heated bundles; and trefoil dryout tests at high pressure and temperatures ranging from 320 to 600 °C at the Stern Laboratories. However, these various tests and experiments were not carried out with prototypic bundles or the experimental conditions were not necessarily prototypic of accident transients. Thus, additional experiments on fuel bundle deformation are needed up to and above 600 °C for development and validation of the various simulation tools.

The ELESTRES code is currently used to determine CANDU fuel performance during normal operating conditions [12,13]. For transient calculations, the ELOCA code [14] employs the steady-state results from the ELESTRES code as initial conditions to determine fuel behaviour for high-temperature transient analysis. A similar strategy is also used for LWR analysis with the FRAPCON code [4] for normal operation prediction and the FRAPTRAN code [5] for transient analysis. However, it would be advantageous to have a single code to cover all such conditions. For example, the European TRANSURANUS code was designed to handle both normal and transient analysis in a single code [7]. Moreover, an extension of these various codes for multi-dimensional capability may be especially needed to simulate the full bundle behaviour with the possibility of local element-to-element and element-to-pressure tube contact.

Finally, current and emerging trends in fuel modelling are underway to better quantify the uncertainties in the models, empirical correlations and input data, and to improve the understanding of high-burnup structures in oxide fuels and the behaviour of advanced fuels [1]. On-going experiments are expensive to undertake. As such, international efforts are also focusing on the simulation of fundamental fuel properties and behaviour involving ab initio, molecular dynamics, Monte Carlo, phase-field, thermal–chemical and finite-element analysis, which entail a multi-scale approach at the: (i) electronic structural level (i.e. stability and elastic constants), (ii) atomic scale (i.e. defect formation, free energies and irradiation effects), (iii) meso-scale (i.e. fuel microstructural evolution and species mobility), and (iv) continuum scale (i.e. thermomechanical properties) [285].

3. Conclusions

An overview of phenomena associated with high-temperature fuel behaviour is presented. The paper addresses the generation of heat from fission and chemical processes. The important thermophysical properties of the fuel (e.g. thermal conductivity, heat capacity, fuel expansion, and the incipient melting temperature of the fuel) that affect heat transport are reviewed. The effect of physical restructuring in the fuel (e.g. fuel porosity, fuel densification, grain growth, gas bubble formation, fuel cracking and relocation) is addressed. The physical and chemical influences of the sheath (i.e. sheath deformation, oxidation and hydriding), as well as the impact of these phenomena on fuel/sheath heat transfer and fuel/sheath interaction, are discussed. The criteria for sheath failure in accordance with high-temperature fuel behaviour are examined. Finally, the response of the fuel/fuel element/bundle during power pulse (e.g. with the possibility of fuel fragmentation) and the deformation of the fuel bundle during severe reactor conditions are detailed.

Acknowledgements

This work is a compilation of the extensive reviews and knowledge on high-temperature fuel behaviour provided by H.E. Sills, M.J.F. Notley, Y. Liu, V.J. Langman and J. Luxat. The authors would like to express their thanks and acknowledge the significant effort provided by these authors.

References

[1] P. Van Uffelen, Modelling of nuclear fuel behaviour, European Commission Directorate – General Joint Research Centre Institute for Transuranium Elements, EUR 22321 EN ISSN 1018–5593, 2006.
[2] R. Godesar, M. Guyette, N. Hoppe, Nucl. Appl. Technol. 9 (1970) 205–217.
[3] E. Bonnaud, C. Bernard, E. Van Schel, Trans. Am. Nucl. Soc. 77 (1997).
[4] G.A. Berna, C.E. Beyer, K.L. Davis, D.D. Lanning, FRAPCON-3: a computer code for the calculation of steady-state, thermal–mechanical behaviour of oxide fuel rods for high burnup, NUREG/CR-6534, PNNL-11513, December 1997.
[5] M.E. Cunningham, C.E. Beyer, P.G. Medvedev, G.A. Berna, FRAPTRAN: a computer code for the transient analysis of oxide fuel rods, NUREG/CR-6739, PNNL-13576, vol. 1, 2001.
[6] M. Uchida, N. Otsubo, Models of multi-rod code FRETA-B for transient fuel behaviour analysis (final version), JAERI 1293, November 1984.
[7] K. Lassmann, J. Nucl. Mater. 188 (1992) 295–302.
[8] J.P. Van Dorsselaere, J.C. Micaelli, H.J. Allelein, ASTEC and SARNET – integrating severe accident research in Europe, in: International Congress on Advances in Nuclear Power Plants (ICAPP'05), Seoul, May 15–19, 2005.
[9] R.O. Gauntt, R.K. Cole, C.M. Erickson, R.G. Gido, R.-D. Gasser, S.B. Rodrigez, M.F. Young, MELCOR computer code manuals, version 1.8.5, May 2000, NUREG/CR-6119, SAND-2417/2, May 2000.
[10] S.S. Dosanjh (Ed.), MELPROG-PWR/MOD1: A Two-Dimensional, Mechanistic Code for Analysis of Reactor Core Melt Progression and Vessel Attack under Severe Accident Conditions, Sandia National Laboratories, NUREG/CR-5193, SAND88-1824, May 1989.
[11] G.A. Berna et al., RELAP5/SCDAP/MOD0 code manual, EGG-RTH-7051, EG&G, September1985.
[12] M. Tayal, Modelling CANDU fuel under normal operating conditions, ELESTRES code description, AECL Report 9331, February 1987.
[13] K.S. Sim, G.G. Chassie, Z. Xu, M. Tayal, C. Westbye, Progress in qualifying ELESTRES-IST 1.0 code: verification and interim results of validation, in: Seventh CNS International Conference on CANDU Fuel, Kingston, Ontario, Canada, September 23–27, 2001, pp. 21–33 (5B).
[14] H.E. Sills, ELOCA fuel element behaviour during high-temperature transients, AECL Report AECL-6357, 1979.
[15] A.F. Williams, The ELOCA fuel modelling code: past, present and future, in: Ninth International CNS Conference on CANDU Fuel, Belleville, Ontario, Canada, September 18–21, 2005.
[16] B.J. Lewis, R. Dickson, F.C. Iglesias, G. Ducros, T. Kudo, J. Nucl. Mater. 380 (2008) 126–143.
[17] M.J.F. Notley, Nucl. Technol. 44 (1979) 445–450.
[18] J.A.L. Roberston, $\int k d\theta$ in fuel irradiations, AECL-807, 1959.
[19] K. Lassmann, C. O'Carroll, J. Nucl. Mater. 208 (1994) 223–231.
[20] K. Lassmann, C.T. Walker, J. Nucl. Mater. 255 (1998) 222–233.
[21] M. Tayal, Eng. Des. 114 (1989) 99–114.
[22] P.M. French, Measurements of bundle end flux peaking effects in 37 element CANDU PHW fuel, Atomic Energy of Canada Limited Report AECL-5968, October 1977.
[23] M.H.M. Roshd, H.C. Chow, The analysis of flux peaking at nuclear fuel bundle ends using PEAKAN, Atomic Energy of Canada Limited Report AECL-6174, April 1978.
[24] M.J.F. Notley, Encyclopaedia of CANDU fuel under normal operating conditions, Ontario Hydro Report, File 906-N-03500 P, COG-88-171, November 1988.
[25] P.E. MacDonald, L.B. Thompson, MATPRO – version 09, a handbook of material properties for use in the analysis of light water reactor fuel rod behavior, USNRC Report TREE-NUREG-1005, December 1976.
[26] D.L. Hagrman, G.A. Reymann, MATPRO – version 11 – a handbook of materials properties for use in the analysis of light water fuel rod behaviour, US Nuclear Regulatory Commission and US Department of Energy, NUREG/CR-0497, TREE-1280, February 1979 and August 1981 (REV. 2).
[27] SCDAP/RELAP5 Development Team, SCDAP/RELAP5/MOD3.2 Code Manual; vol. IV: MATPRO – A Library of Materials Properties for Light-Water Reactor Accident Analysis, NUREG/CR-6150, vol. IV (INEL-96/0422), REV. 1, October 1997.
[28] SCDAP/RELAP5-3D Code Manual Volume 4: MATPRO – A Library of Materials Properties for Light – Water Reactor Accident Analysis, INEEL/EXT-02-00589, vol. 4, Revision 2.2, October 2003.
[29] International Atomic Energy Agency, Thermophysical properties of materials for water-cooled reactors, IAEA-TECDOC-949, June 1997.
[30] J.K. Fink, J. Nucl. Mater. 279 (2000) 1–18.
[31] J. Carbajo, G. Yoder, S. Popov, V. Ivanov, J. Nucl. Mater. 299 (2001) 181.
[32] D.R. Olander, Fundamental aspects of nuclear reactor fuel elements, TID-26711-p1, US Department of Energy, 1976.
[33] P.G. Lucuta, H.J. Matzke, R.A. Verrall, H.A. Tasman, J. Nucl. Mater. 188 (1992) 198–204.
[34] J.H. Harding, D.G. Martin, J. Nucl. Mater. 166 (1989) 223–226.
[35] P.G. Lucuta, H.J. Matzke, I.J. Hastings, J. Nucl. Mater. 232 (1996) 166–180.
[36] L.A. Goldsmith, J.A.M. Douglas, UKAEA Report TGR 2103(w), 1971.
[37] W. Wiesenack, Thermal performance of high burnup fuel – in-pile temperature data and analysis, Light Water Reactor Fuel Performance Conference, Portland, Oregon, March 2–6, 1997, p. 507.
[38] W. Wiesenack, T. Tverberg, Assessment of UO_2 conductivity degradation based on in-pile temperature data, Light Water Reactor Fuel Performance Conference, Park City, Utah, April 10–13, 2000.
[39] C. Ronchi, M. Sheindlin, M. Musella, G.J. Hyland, J. Appl. Phys. 85 (1999) 776–789.
[40] M. Amaya, M. Hirai, J. Nucl. Mater. 247 (1997) 76–81.
[41] C. Ronchi, M. Sheindlin, D. Staicu, M. Kinoshita, J. Nucl. Mater. 327 (2004) 58–76.
[42] B.J. Lewis, B. Szpunar, F.C. Iglesias, J. Nucl. Mater. 306 (2002) 30.
[43] B.J. Lewis, W.T. Thompson, F. Akbari, D.M. Thompson, C. Thurgood, J. Higgs, J. Nucl. Mater. 328 (2004) 180–196.
[44] J.D. Higgs, B.J. Lewis, W.T. Thompson, Z. He, J. Nucl. Mater. 366 (2007) 99–128.
[45] J.D. Higgs, B.J. Lewis, W.T. Thompson, The significance of thermal conductivity on nuclear fuel oxidation modelling, in: 28th International Thermal Conductivity Conference (ITCC), St. Andrew's, New Brunswick Canada, June 26–29, 2005.
[46] J.C. Ramirez, M. Stan, P. Cristea, J. Nucl. Mater. 359 (2006) 174–184.
[47] W.E. Ellis, J.D. Porter, T.L. Shaw, The effect of oxidation, burnup and poisoning on the thermal conductivity of UO_2: a comparison of data with theory, in: Proceedings of the International Topical Meeting on Light Water Reactor Fuel Performance, Park City, Utah, April 10–13, 2000, p. 715.
[48] P.G. Lucuta, H.J. Matzke, R.A. Verrall, J. Nucl. Mater. 223 (1995) 51–60.
[49] V.C. Howard, T.F. Gulvin, Thermal conductivity determinations on uranium dioxide by a radial flow method, UKAEA Report, IG Report 51 (RD/c), 1961.
[50] L.A. Goldsmith, J.A.M. Douglas, J. Nucl. Mater. 47 (1973) 31–42.
[51] P.G. Klemens, Phys. Rev. 119 (2) (1960) 507–509.
[52] P.G. Klemens, High Temp. – High Press. 17 (1985) 41–45.
[53] P.G. Klemens, Proc. Phys. Soc. (London) A68 (1955) 1113–1128.
[54] R.A. Gomme, J.C. Carrol, T.L. Shaw, High Temp. – High Press. 30 (1998) 135–140.
[55] M. Amaya, T. Kubo, Y. Korei, J. Nucl. Sci. Technol. 33 (1996) 636–640.
[56] T. Shaw, W.E. Ellis, J.C. Carrol, R.A. Gomme, Thermal diffusivity measurements on oxidised irradiated urania fuel up to 900 °C, in: Proceedings of the Technical Committee Meeting on Nuclear Fuel Behaviour Modelling at High Burnup and its Experimental Support, June 19–23, 2000, Windermere, United Kingdom, IAEA-TECDOC-1233, 2001.
[57] M. Serizawa, H. Kaneko, Y. Yokouchi, M. Koizumi, Thermal conductivity measurement of hypostoichiometric uranium dioxide by a modulated electron beam technique, in: Thermal Conductivity, Eighth Conference, Purdue University, Indiana, USA, 1969, pp. 549–567.
[58] M. Serizawa, H. Kaneko, M. Koizumi, J. Nucl. Sci. Technol. 6 (1969) 419–423.
[59] C. Duriez, J.-P. Alessandri, T. Gervais, Y. Philipponneau, J. Nucl. Mater. 277 (2000) 143–158.
[60] J.F. Kerrisk, D.G. Clifton, Nucl. Technol. 16 (1972) 531–535.
[61] M.T. Hutchings, J. Chem. Soc. Faraday Trans. II 83 (1987) 1083.
[62] J.P. Hiernaut, G.J. Hyland, C. Ronchi, Int. J. Thermophys. 14 (2) (1993) 259–283.
[63] K. Naito, J. Nucl. Mater. 167 (1989) 30–35.
[64] R.A. Verrall, P.G. Lucuta, J. Nucl. Mater. 228 (1996) 251–253.
[65] H.J. Matzke, P.G. Lucuta, R.A. Verrall, J. Henderson, J. Nucl. Mater. 247 (1997) 121–126.
[66] D.G. Martin, J. Nucl. Mater. 152 (1988) 94–101.
[67] W. Breitung, K.O. Reil, Nucl. Sci. Eng. 105 (1990) 205.
[68] C.W. Bale, A.D. Pelton, W.T. Thompson, Facility for the Analysis of Chemical Thermodynamics, McGill University and École Polytechnique, 1995.
[69] P.-Y. Chevalier, E. Fischer, B. Cheynet, J. Nucl. Mater. 303 (2002) 1.
[70] C. Guéneau, M. Baichi, D. Labroche, C. Chatillon, B. Sundman, J. Nucl. Mater. 304 (2002) 161.
[71] F. Akbari, B.J. Lewis, W.T. Thompson, Considerations in the modelling the melting of fuel containing fission products and solute oxides, in: Ninth International Conference on CANDU Fuel, Belleville, Ontario, September 18–21, 2005.
[72] M.H. Kaye, C. Morrison, J.D. Higgs, F. Akbari, B.J. Lewis, W.T. Thompson, Toward a first principles model of CANDU fuel phase equilibrium, in: Ninth International Conference on CANDU Fuel, Belleville, Ontario, September 18–21, 2005.
[73] S. White, F. Akbari, B.J. Lewis, W.T. Thompson, Thermodynamic modelling of UO_2–Ln_2O_3 systems, in: Ninth International Conference on CANDU Fuel, Belleville, Ontario, September 18–21, 2005.
[74] W.T. Thompson, B.J. Lewis, E.C. Corcoran, M.K. Kaye, S.J. White, F. Akbari, Z. He, R. Verrall, J.D. Higgs, D.M. Thompson, T.M. Besmann, S.C. Vogel, Int. J. Mater. Res. 98 (10) (2007) 1004–1011.
[75] D. Manara, C. Ronchi, M. Sheindlin, Int. J. Thermophys. 23 (5) (2002).
[76] D. Manara, C. Ronchi, M. Sheindlin, High Temp. – High Press. 35/36 (2003/2004) 25–33.
[77] D. Manara, M. Sheindlin, Int. J. Thermophys. 25 (2) (2004).

[78] D. Manara, C. Ronchi, M. Sheindlin, M. Lewis, M. Brykin, J. Nucl. Mater. 342 (2005) 148–163.
[79] R.E. Latta, R.E. Fryxell, J. Nucl. Mater. 35 (1970) 195.
[80] F.C. Iglesias, H.E. Sills, Y. Liu, V.J. Langman, M.J.F. Notley, CANDU fuel behaviour during large break LOCA overpower transients, Reactor Safety and Operational Analysis Department, Ontario Hydro Report HIST/RP/1085, August 1993.
[81] K.C. Buschbeck, C. Keller, Chief Editors, Gmelin Handbook of Inorganic Chemistry, Uranium, eighth ed., vol. A4 (Suppl.), 1982.
[82] P.G. Lucuta, R.A. Verrall, H.J. Matzke, J. Nucl. Mater. 223 (1995) 51–60.
[83] I.J. Hastings, L.E. Evans, J. Am. Ceram. Soc. 62 (1979) 217–218.
[84] H. Assmann, H. Stehle, Nucl. Eng. Des. 48 (1977) 49–67.
[85] J.R. Mathews, G.J. Small, Towards a mechanistic understanding of transient fission gas release, in: IAEA Meeting on Water Reactor Fuel Modelling in Steady State, Transient and Accident Conditions, September 1988.
[86] I. Zacharie, S. Lansiart, P. Combette, M. Trotabas, M. Coster, M. Groos, J. Nucl. Mater. 255 (1998) 85–91.
[87] I. Zacharie, S. Lansiart, P. Combette, M. Trotabas, M. Coster, M. Groos, J. Nucl. Mater. 255 (1998) 92–104.
[88] G.J. Small, Fission gas release from uranium dioxide in high temperature transients, UKAEA Harwell Report AERE R 12956, May 1988 (M.Sc. Thesis, University of Birmingham).
[89] R.J. White, The development of grain face porosity in irradiated oxide fuel, in: Proceedings of the OECD NEA Seminar on Fission Gas Behaviour in Water Reactor Fuels, Cadarache, France, September 26–29, 2000, pp. 189–198.
[90] R.J. White, R.C. Corcoran, P.J. Barnes, A summary of swelling data obtained from the AGR/halden ramp test programme, R&T/NG/EXT/REP/0206/02 – Issue 2, March 2003.
[91] K. Une, S. Kashibe, K. Ito, J. Nucl. Sci. Technol. 30 (1993) 221–231.
[92] S. Kashibe, K. Une, K. Nogita, J. Nucl. Mater. 206 (1993) 22–34.
[93] R. Yuda, H. Harada, M. Hirai, T. Hosokawa, K. Une, S. Kashibe, S. Shimizu, T. Kubo, J. Nucl. Mater. 248 (1997) 262–267.
[94] R.M. Cornell, J. Nucl. Mater. 38 (1971) 319–328.
[95] C. Baker, J. Nucl. Mater. 66 (1977) 283–291.
[96] H. Zimmermann, J. Nucl. Mater. 75 (1978) 154–161.
[97] M.J.F. Notley, I.J. Hastings, A microstructure-dependent model for fission product gas release and swelling in UO_2 fuel, AECL-5838, 1978.
[98] A.S. Bain, Cracking and bulk movement in irradiated uranium oxide fuel elements, AECL-1827, 1963.
[99] K. Une, S. Kashibe, J. Nucl. Sci. Technol. 27 (11) (1990) 1002–1016.
[100] S. Kashibe, K. Une, Nucl. Sci. Technol. 28 (12) (1991) 1090–1099.
[101] J. Rest, Nucl. Technol. 56 (1982) 553–564.
[102] R.J. DiMelfi, L.W. Deitrich, Nucl. Technol. 43 (1979) 328.
[103] T. Chuang, K.I. Kawaga, J.M. Rice, L.B. Sills, Acta Metall. 27 (1978) 265–284.
[104] C.R. Kennedy, R.A. Christensen, R.F. Eibert, UO_2 pellet fragment relocation: kinetics and mechanics, EPRI NP-1 106, 1979.
[105] J.C. Wood, B.A. Surette, I. Aitchinson, W.R. Clendenning, J. Nucl. Mater. 88 (1980) 81.
[106] A.M. Ross, R.L. Stoute, Heat transfer between UO_2 and zircaloy-2, AECL-1552, 1962.
[107] D.D. Lanning, Nucl. Technol. 56 (1982) 565–574.
[108] P.J. Fehrenbach, P.A. Morel, R.D. Sage, Nucl. Technol. 56 (1982) 112–119.
[109] R.D. MacDonald, D.C. Card, Irradiation of UO_2–zircaloy fuel elements with free-standing cladding and large diametral clearances, AECL-5119, 1975.
[110] A.S. Bain, Irradiation of UO_2 specimens with molten cores in a pressurized water loop, AECL Report AECL-1464, August 1961.
[111] B.J. Lewis, F.C. Iglesias, D.S. Cox, E. Gheorghiu, Nucl. Technol. 92 (1990) 353–362.
[112] W. Hüttig, H. Zänker, M. Forberg, J. Nucl. Mater. 175 (1990) 147–157.
[113] B.J. Lewis, W.T. Thompson, F. Akbari, C. Thurgood, A fuel oxidation model for operating defective fuel elements, COG 02-2122, April 2003.
[114] M.J. Welland, J. Nucl. Mater. 376 (2008) 229–239.
[115] M.J. Welland, W.T. Thompson, B.J. Lewis, D. Manara, J. Nucl. Mater. 385 (2009) 358–363.
[116] H.E. Sills, R.A. Holt, NIRVANA, a high-temperature creep model for zircaloy fuel sheathing, AECL Report AECL-6412, 1979, pp. 209–220.
[117] Y. Suh, D. Sohn, J. Kor. Nucl. Soc. 20 (1988) 191.
[118] F.R. Campbell, L.R. Bourque, R. Deshaies, H. Sills, M.J.F. Notley, In-reactor measurements of the fuel-to-sheath heat transfer coefficients between UO_2 and stainless steel, AECL Report AECL-5400, May 1977.
[119] J.A. Walsworth, H.E. Sills, S. Sagat, Failure criteria for zircaloy-sheath fuel elements under LOCA conditions, in: Proceedings of the Canadian Nuclear Society Sixth Annual Conference, June 1985, pp. 11.7–11.13.
[120] V.I. Arimescu, M.E. Klein, J.R. Gauld, Z.W. Lian, L.N. Carlucci, Evolution of the ELOCA code: Mk6 to the present, in: Fifth International Conference on CANDU Fuel, Toronto, Ontario, September 21–25, 1997.
[121] C.E.L. Hunt, The limit of uniform strain, or onset of ballooning, in fuel sheath ballooning tests, Atomic Energy of Canada Limited Report CRNL-1187, September 1974.
[122] D.G. Hardy, High temperature expansion and rupture behaviour of zircaloy tubing, in: National Topical Meeting on Water Reactor Safety, Salt Lake City, Utah, CONF-730304, 1973, p. 254.
[123] D.G. Hardy, A.S. Bain, ASTM-STP 633 (1977) 98.
[124] A. Sawatzky, A proposed criterion for the oxygen embrittlement of zircaloy-4 fuel cladding, in: Fourth International Conference on Zirconium in the Nuclear Industry, Stratford-upon-Avon, 1978, pp. 479–496.
[125] S. Sagat, H.E. Sills, J.A. Walsworth, D.E. Foote, D.F. Shields, Deformation and failure of zircaloy fuel sheaths under LOCA conditions, in: Sixth International Conference on Zirconium in the Nuclear Industry, Vancouver, Canada 1982 June 28–July 01 (also AECL-7754, 1982).
[126] D.R. Olander, Nucl. Eng. Des. 148 (1994) 253–271.
[127] C.M. Allison et al., Capabilities of the integrated SCDAP/RELAP5/TRAP-MELT severe accident computer code, in: Proceedings of the IAEA International Symposium on Source Term Evaluation for Accident Conditions, Columbus, OH, 1985.
[128] Fauske and Associates, MAAP3.0B computer code manual, EPRI Rep. NE-7071-CCML, November 1990.
[129] T.J. Heames et al., VICTORIA, a mechanistic model of radionuclide behavior in the reactor coolant system under severe accident conditions, Rep. NUREG CR-5545, 1990.
[130] L. Baker, L.C. Just, Studies of metal–water reactions at high temperatures, Rep. ANL-6548, Argonne National Laboratory, Argonne, IL, 1962.
[131] V.F. Urbanic, T.R. Heidrick, J. Nucl. Mater. 75 (1978) 251–261 (also AECL Report AECL-6149).
[132] J.T. Prater, E.L. Courtwright, Oxidation of zircaloy-4 in steam at 1300–2400 °C, in: Proceedings of the Seventh International Symposium on Zirconium in the Nuclear Industry, ASTM Spec. Tech. Publ., vol. 939, 1987, p. 489.
[133] R.E. Pawel, J. Electrochem. Soc. 126 (1979) 1111.
[134] G. Schanz, B. Adroguer, A. Volchek, Nucl. Eng. Des. 232 (1) (2004) 75–84.
[135] A. Volchek, Yu. Zvonarev, G. Schanz, Nucl. Eng. Des. 232 (1) (2004) 85–96.
[136] F. Fichot, B. Adroguer, A. Volchek, Yu. Zvonarev, Nucl. Eng. Des. 232 (1) (2004) 97–109.
[137] B.J. Lewis, D.S. Cox, F.C. Iglesias, J. Nucl. Mater. 207 (1993) 228–241.
[138] R.E. Pawel, J.V. Cathcart, J.J. Campbell, J. Nucl. Mater. 82 (1) (1979) 129–139.
[139] K. Park, Y. Taegeun, K. Sungkwon, H.G. Kim, Y. Jeong, K. Kim, High temperature oxidation of zirconium base alloy in steam, in: Seventh International CANDU Fuel Conference, Kingston, Ontario (Canada) 23–27 September 2001, ISBN 0-919784-71-2, vol. 2, pp. 3B.1–3B.10.
[140] T. Furuta, S. Kawasaki, J. Nucl. Mater. 105 (2/3) (1982) 119–131.
[141] F.C. Iglesias, D.B. Duncan, S. Sagat, H.E. Sills, J. Nucl. Mater. 130 (1985) 3644.
[142] S. Malang, SIMTRAN I-A compute code for the simultaneous calculation of oxygen distributions and temperature profiles in zircaloy during exposure to high-temperature oxidizing environments, Rep. ORNL-5083, Oak Ridge National Laboratory, Oak Ridge, TN, 1975.
[143] P. Hofmann, H.J. Neitzel, Experimental and theoretical results of cladding oxidation under severe fuel-damage conditions, in: Seventh Symposium, ASTM STP, vol. 939, 1987, pp. 504–538.
[144] J.J. Vermoyal, L. Dessemond, A. Hammou, A. Frichet, J. Nucl. Mater. 298 (3) (2001) 297–308.
[145] C. Duriez, T. Dupont, B. Schmet, F. Enoch, Zircaloy-4 and M5 high temperature oxidation and nitriding in air, J. Nucl. Mater. 380 (2008) 30–45.
[146] M. Suzuki, S. Kawasaki, J. Nucl. Mater. 140 (1) (1986) 32–43.
[147] Z. Hozer, L. Maroti, P. Windberg, L. Matus, I. Nagy, G. Gyenes, M. Horvath, A. Pinter, M. Balasko, A. Czitrovszky, P. Jani, A. Nagy, O. Prokopiev, B. Toth, Nucl. Technol. 154 (2006) 302–317.
[148] M. Steinbrück, J. Nucl. Mater. 392 (2009) 531–544.
[149] T. Furuta, H. Uetsuka, S. Kawasaki, J. Nucl. Sci. Technol. 18 (10) (1981) 802–810.
[150] H. Uetsuka, T. Furuta, S. Kawasaki, J. Nucl. Sci. Technol. 18 (9) (1981) 705–717.
[151] H. Uetsuka, T. Furuta, S. Kawasaki, J. Nucl. Sci. Technol. 20 (11) (1983) 941–950.
[152] F. Nagase, T. Fuketa, J. Nucl. Sci. Technol. 41 (7) (2004) 723–730.
[153] F. Nagase, T. Fuketa, J. Nucl. Sci. Technol. 42 (2) (2005) 209–218.
[154] J.H. Kim, M.H. Lee, B.K. Choi, Y.H. Jeong, Nucl. Eng. Des. 235 (1) (2005) 67–75.
[155] S.M. Jensen, D.W. Akers, B.A. Pregger, Postirradiation examination data and analysis for OECD LOFT fission product experiment LP-FP-2, OECD LOFT-T-3810, Organization of Economic Cooperation and Development, vol. 1, December 1989.
[156] R.R. Hobbins, G.D. McPherson, in: Proceedings of the Open Forum on the OECD/LOFT Project, Achievements and Significant Results, Madrid, Spain, 9–11 May 1990, Organization of Economic Cooperation and Development, 1991.
[157] D.R. Olander, Nucl. Eng. Des. 148 (1994) 273–292.
[158] B.J. Lewis, J. Nucl. Mater. 279 (1999) 221–232.
[159] B. Szpunar, B.J. Lewis, V.I. Arimescu, R.S. Dickson, L.W. Dickson, J. Nucl. Mater. 294 (2001) 315–329.
[160] G. Boureau, P. Gerdanian, Can. Metall. Quart. 13 (1974) 339.
[161] G. Boureau, P. Gerdanian, J. Phys. Chem. Solids 4 (1984) 141.
[162] D.R. Olander, Pure Appl. Chem. 67 (6) (1995) 1003–1010.
[163] O. Kubaschewski, Zirconium: physico-chemical properties of its compounds and alloys, IAEA Special Issue 6, 1976.
[164] M. Moalem, D.R. Olander, J. Nucl. Mater. 178 (1991) 61.
[165] K.H. Park, D.R. Olander, J. Am. Ceram. Soc. 74 (1991) 72.
[166] S. Yamanaka, K. Higuchi, M. Miyake, J. Alloys Compd. 231 (1995) 503–507.
[167] M. Steinbrück, J. Nucl. Mater. 334 (2004) 58–64.
[168] W. Dienst, P. Hofmann, D. Kerwin-Peck, Nucl. Technol. 65 (1984) 109.
[169] W.G. Hutchings, H.E. Rosinger, The UO_2/zircaloy interaction: a metallographic examination, in: Proceedings of the ASM Metals Congress, Detroit, IL, 1984.
[170] H.E. Rosinger, R.K. Rondeau, K. Demoline, K.J. Ross, The interaction and dissolution of solid UO_2 by molten zircaloy-4 cladding in an inert atmosphere

or steam, in: Sixth Annual Conference of the Canadian Nuclear Society, Ottawa, Ontario, June 3–4, 1985, p. 16.33.
[171] P. Hofmann, H. Uetsuka, A.N. Wilhelm, E.A. Garcia, Dissolution of solid UO_2 by molten zircaloy and its modelling, in: IAEA/OECD International Symposium on Severe Accidents in Nuclear Power Plants, Sorrento, Italy, March 21–25, 1988 (IAEA-SM-296/99), p. 3.
[172] P. Nikolopoulos, P. Hofmann, D.K. Kerwin-Peck, J. Nucl. Mater. 124 (1984) 106.
[173] K.Y. Kim, D.R. Olander, J. Nucl. Mater. 154 (1988) 85.
[174] P.J. Hayward, I.M. George, J. Nucl. Mater. 208 (1994) 35.
[175] P.J. Hayward, I.M. George, J. Nucl. Mater. 208 (1994) 43.
[176] D.R. Olander, J. Nucl. Mater. 224 (1995) 254.
[177] P.J. Hayward, I.M. George, J. Nucl. Mater. 232 (1996) 1.
[178] P.J. Hayward, I.M. George, J. Nucl. Mater. 232 (1996) 13.
[179] M.S. Veshchunov, P. Hofmann, A.V. Berdyshev, J. Nucl. Mater. 231 (1996) 1.
[180] D.R. Olander, Nucl. Eng. Des. 162 (1996) 257–270.
[181] P.J. Hayward, P. Hofmann, J. Stuckert, M.S. Veshchunov, A.V. Berdyshev, UO_2 dissolution by molten zircaloy. New experimental results and modelling, FzK Report FZKA-6379/INV-CIT-99-P029, December 1999.
[182] P.J. Hayward, I.M. George, J. Nucl. Mater. 265 (1999) 69–77.
[183] P. Hofmann, J. Stuckert, A. Miassoedov, M.S. Veshchunov, A.V. Berdyshev, A.V. Boldyrev, ZrO_2 dissolution by molten zircaloy and cladding oxide shell failure. New experimental results and modelling, FzK Report FZKA-6383/INV-CIT-98-P026, December 1999 (in English).
[184] K. Mueller, A.V. Goryachev, V.P. Smirnov, A.M. Svyatkin, J. Stuckert, M.S. Veshchunov, A.V. Berdyshev, Simultaneous dissolution of UO_2 and ZrO_2 by molten zircaloy. New experiments and modelling, FzK/EU Report FZKA-6947/SAM-COLOSS-P-074, January 2004.
[185] J. Stuckert, A. Miassoedov, P.J. Hayward, P. Hofmann, M. Veshchunov, ZrO_2 and UO_2 dissolution by molten zircalloy, in: Proceedings of the International Conference Nuclear Energy in Central Europe 2002, Kranjska Gora, Slovenia, September 9–12, 2002, p. 8 (electronic).
[186] B. Adroguer, F. Bertrand, P. Chatelard, N. Cocuaud, J.P. Van Dorsselaere, L. Bellenfant, D. Knocke, D. Bottomley, V. Vrtilkova, L. Belovsky, K. Mueller, W. Hering, C. Homann, W. Krauss, A. Miassoedov, G. Schanz, M. Steinbrueck, J. Stuckert, Z. Hozer, G. Bandini, J. Birchley, T. von Berlepsch, I. Kleinhietpass, M. Buck, J.A.F. Benitez, E. Virtanen, S. Marguet, G. Azarian, A. Caillaux, H. Plank, A. Boldyrev, M. Veshchunov, V. Kobzar, Y. Zvonarev, A. Goryachev, Nucl. Eng. Des. 235 (2–4) (2005) 173–198.
[187] Y. Pontillon, P.P. Malgouyres, G. Ducros, G. Nicaise, R. Dubourg, M. Kissane, M. Baichi, J. Nucl. Mater. 344 (2005) 265–273.
[188] T. Kudo, T. Nakamura, M. Kida, T. Fuketa, Enhancement of cesium release from fuel due to fuel oxidation and dissolution under severe accident conditions, in: Technical Meeting on Severe Accident and Accident Management, Tokyo, Japan, March 14–16, 2006.
[189] M.F. Osborne, R.A. Lorenz, J.L. Collins, J.R. Travis, C.S. Webster, T. Nakamura, Data summary report for fission product release test VI-4, USNRC/ORNL Report NUREG/CR-5481/ORNL/TM-11400, January 1991.
[190] M.F. Osborne, R.A. Lorenz, J.R. Travis, C.S. Webster, J.L. Collins, Data summary report for fission product release test VI-5, USNRC/ORNL Report NUREG/CR-5886/ORNL/TM-11743, October 1991.
[191] P.D.W. Bottomley, J.-P. Glatz, M. Barrachin, Irradiated UO_2 fuel dissolution by molten zircaloy. Some results from the SCA corium interaction thermochemistry project, in: Proceedings of the SARJ-99 Workshop on Severe Accident Research, Tokyo, Japan, 1999 November 8–10, JAERI-Conference 2000–2015, pp. 123–129.
[192] J.C. Luxat, Fuel behaviour during a power pulse: a review and assessment of reactivity initiated accident test data, in: Proceedings of the CNS Annual Conference, Toronto, June 2002.
[193] J.C. Luxat, Analytical criteria for fuel failure modes observed in reactivity initiated accidents, in: Proceedings of the 26th Annual CNS Conference, June 2005.
[194] P.E. MacDonald, S.L. Seiffert, Z.R. Martinson, R.K. McCardell, D.E. Owen, S.K. Fukuda, Nucl. Safety 21 (5) (1980).
[195] S. Katanishi, K. Ishijima, J. Nucl. Sci. Technol. 32 (11) (1995).
[196] T. Fujishiro, K. Yanagisawa, K. Ishijima, K. Shiba, J. Nucl. Mater. 188 (1992).
[197] K. Yanagisawa, Nucl. Eng. Des. 116 (1989).
[198] K. Ishijima, T. Nakamura, J. Nucl. Sci. Technol. 33 (3) (1996).
[199] S. Saito, K. Ishijima, S. Shiozawa, K. Iwata, J. Nucl. Sci. Technol. 19 (4) (1982).
[200] T. Abe, N. Nakae, K. Kodato, M. Matsumoto, T. Inabe, J. Nucl. Mater. 188 (1992).
[201] S. Yanagihara, S. Shiozawa, J. Nucl. Sci. Technol. 24 (11) (1987).
[202] S. Shiozawa, S. Saito, S. Yanagihara, J. Nucl. Sci. Technol. 19 (5) (1982).
[203] T. Fujishiro, M. Hirose, S. Kobayashi, S. Tanzawa, J. Nucl. Sci. Technol. 18 (3) (1981).
[204] T. Fuketa, K. Ishijima, T. Fujishiro, J. Nucl. Sci. Technol. 33 (1) (1996).
[205] NSRR Experimental Research Results, 16th NSRR Technical Review Meeting, Reactivity Accident Laboratory, JAERI, November 2–3, 1992.
[206] T. Sugiyama, T. Fuketa, J. Nucl. Sci. Technol. 37 (10) (2000).
[207] T. Fuketa, T. Fujishiro, Nucl. Eng. Des. 146 (1994).
[208] L. Yegorova, Data base on VVER high burn-up fuel rods under RIA conditions: final report, COG Report COG-96-548, vols. 1 and 2, October 1996.
[209] V. Asmolov, L. Yegorova, Development and performance of a research program for the analysis of high burn-up fuel rod behavior under RIA conditions in the IGR pulse reactor, in: Proc. CSNI Spec. Mtg. on Transient Behavior of High Burnup Fuel, Cadarache, France, September 12–14, 1995.
[210] V. Asmolov, L. Yegorova, Results of reactor tests to investigate VVER fuel element behavior under RIA conditions, COG Report COG-97-290-E, June 1996.
[211] J. Papin, M. Balourdet, F. Lemoine, J.M. Frizonnet, F. Schmitz, Nucl. Safety 37 (1996).
[212] J. Papin, H. Rigat, J.P. Breton, The behaviour of irradiated fuel under RIA transients: interpretation of the CABRI experiments, in: Proc. CSNI Spec. Mtg. on Transient behavior of High Burnup Fuel, Cadarache, France, September 12–14, 1995.
[213] F. Schmitz, J. Papin, J. Nucl. Mater. 270 (1999).
[214] G. Negut, M. Popov, J. Nucl. Mater. 188 (1992).
[215] G. Horhoianu, D.V. Ionescu, I. Stefan, G. Olteanu, Nucl. Eng. Des. 179 (1998).
[216] J. Adams, R.K. McCardell, P. Kalish, R. McCormick, Z.R. Martinson, PBF-CANDU fuel element loss-of-coolant accident experiment test results report, EG&G Idaho, Inc., EGG-2384, May 1985.
[217] R.J. DiMelfi, J.M. Kramer, Nucl. Technol. 62 (1983) 51.
[218] H.J. Matzke, J. Spino, J. Nucl. Mater. 248 (1997) 170–179.
[219] P. Hofmann, S.J.L. Hagen, G. Schanz, A. Skokan, Nucl. Technol. 87 (1989) 146.
[220] P. Hofmann, J. Nucl. Mater. 270 (1999) 194.
[221] M.D. Allen, H.W. Stockman, K.O. Reil, A.J. Grimley, W.J. Camp, ACRR fission product release tests ST-1 and ST-2, in: Proc. Int. Conf. Thermal Reactor Safety, vol. 5, Avignon, France, October 2–7, 1988.
[222] R.D. Gasser, C.P. Fryer, R.O. Gauntt, A.C. Marshall, K.O. Reil, K.T. Stalker, Damaged fuel relocation experiment DF-1: results and analyses, NUREG/CR-4668, SAND86-1030, US Nuclear Regulatory Commission, January 1990.
[223] K.O. Reil, A.C. Marshall, R.O. Guantt, R.W. Ostensen, P.S. Pickard, C. Fryer, K.T. Stalker, Results of the ACRR-DFR experiments, in: Proc. Int. Topl. Mtg. Thermal Reactor Safety, vol. 3, American Nuclear Society, San Diego, California, February 2–6, 1986.
[224] R.O. Gauntt, R.D. Gasser, L.J. Ott, The DF-4 fuel damage experiment in ACRR with a BWR control blade and channel box, NUREG/CR-4671, SAND86-1443, US Nuclear Regulatory Commission, November 1989.
[225] A.D. Knipe, S.A. Ploger, D.J. Osetek, PBF severe ful damage scoping test – test results report, NUREG/CR-4683, US Nuclear Regulatory Commission, March 1986.
[226] Z.R. Martinson, D.A. Petti, B.A. Cook, PBF severe fuel damage test 1–1 test results report, NUREG/CR-4684, EGG-2463, vol. 1, US Nuclear Regulatory Commission, October 1986.
[227] Z.R. Martinson, M. Gasparini, R.R. Hobbins, D.A. Petti, C.M. Allison, J.K. Hohorst, D.L. Hagrman, K. Vinjamuri, PBF severe fuel damage test 1–3 test results report, NUREG/CR-5354, EGG-2565, US Nuclear Regulatory Commission, October 1989.
[228] D.A. Petti, Z.R. Martinson, R.R. Hobbins, C.M. Allison, E.R. Carlson, D.L. Hagrman, T.C. Cheng, J.K. Hartwell, K. Vinjamuri, L.J. Seifken, Power burst facility (PBF) severe fuel damage test 1–4 test results report, NUREG/CR-5163, EGG-2542, US Nuclear Regulatory Commission, April 1989.
[229] D.A. Petti, Z.R. Martinson, R.R. Hobbins, D.J. Osetek, Nucl. Technol. 94 (1991) 313.
[230] W.N. Rausch, G.M. Hesson, J.P. Pilger, L.L. King, R.L. Goodman, Coolant boilaway and damage progression program data report: full-length high temperature experiment 1, PNL-5691, Pacific Northwest Laboratories, September 1986.
[231] N.J. Lombardo, D.D. Lanning, F.E. Panisko, Coolant boilaway and damage progression program data report: full-length high temperature experiment 2, PNL-6551, Pacific Northwest Laboratories, April 1988.
[232] D.D. Lanning, N.J. Lombardo, D.E. Fitzsimmons, W.K. Hensley, F.E. Panisko, Coolant boilaway and damage progression program data report: full-length high temperature experiment 4, PNL-6368, Pacific Northwest Laboratories, January 1988.
[233] D.D. Lanning, N.J. Lombardo, D.E. Fitzsimmons, W.K. Hensley, F.E. Panisko, Coolant boilaway and damage progression program data report: full-length high temperature experiment 5, PNL-6540, Pacific Northwest Laboratories, April 1988.
[234] M.L. Carboneau, V.T. Berta, M.S. Modro, Experiment analysis and summary report for OECD LOFT project fission product experiment LP-FP-2, OECD LOFT-T-3806, Organization for Economic Cooperation and Development, June 1989.
[235] J.M. Broughton, P. Kuan, D.A. Petti, E.L. Tolman, Nucl. Technol. 87 (1989) 34.
[236] P. von der Hardt, A. Tattegrain, J. Nucl. Mater. 188 (1992) 115.
[237] P. von der Hardt, A. Jones, C. Lecomte, A. Tattegrain, Nucl. Safety 35 (1994) 2.
[238] M. Schwarz, G. Hache, P. von der Hardt, Nuc. Eng. Des. 187 (1999) 47.
[239] N. Hanniet, G. Repetto, Phebus PF, FPT0 – final report, CD Version, Suntech 10/99.
[240] J. Bonnin, B. Berthet, S. Bayle, N. Hanniet, F. Jeury, S. Gaillot, Y. Garnier, C. Martin, M. Laurie, B. Siri, Phebus PF, FPT1 – preliminary report, IPSN/DRS/SEA/LERES/97/727, Note Technique LERES No. 24/97, Document Phebus PF IP/97/334, October 1997.
[241] P. Hofmann, S.J.K. Hagen, V. Noack, G. Schanz, L.K. Sepold, Nucl. Technol. 118 (1997) 200.
[242] M.F. Osborne, J.L. Collins, R.A. Lorenz, Nucl. Technol. 78 (1987) 157.
[243] M.F. Osborne, R.A. Lorenz, Nucl. Safety 33 (1992) 344.
[244] J.P. Leveque, B. Andre, G. Ducros, G. Le Marois, G. Lhiaubet, Nucl. Technol. 108 (1994) 33.

[245] B. Andre, G. Ducros, J.P. Leveque, D. Maro, M.F. Osborne, R.A. Lorenz, Nucl. Technol. 114 (1996) 23.
[246] B.J. Lewis, B. Andre, B. Morel, P. Dehaudt, D. Maro, P.L. Purdy, D.S. Cox, F.C. Iglesias, M.F. Osborne, R.A. Lorenz, J. Nucl. Mater. 227 (1995) 83.
[247] D.A. Petti, Nucl. Technol. 84 (1989) 128.
[248] R.R. Hobbins, D.A. Petti, D.J. Osetek, D.L. Hagrman, Nucl. Technol. 95 (1991) 287.
[249] A.W. Cronenberg, Nucl. Technol. 93 (1991) 221.
[250] A.W. Cronenberg, Nucl. Technol. 97 (1992) 97.
[251] R.R. Hobbins, D.A. Petti, D.L. Hagrman, Nucl. Technol. 101 (1993) 270.
[252] D.A. Petti, R.R. Hobbins, D.L. Hagrman, Nucl. Technol. 105 (1994) 334.
[253] J. Langman, K.R. Weaver, An overview of the Canadian and international R&D programs related to core behaviour in large break loss-of-coolant accidents with potentially delayed emergency coolant injection, in: International Development and Energy Assessment Report (IDEA), INFO-0114, September 1983.
[254] J. Veeder, M.H. Shankula, Nucl. Eng. Des. 29 (1974) 167–179 (also AECL-4875).
[255] A.W.L. Segel, H. Hatton, V.J. Langman, A model to relate hot and cold fuel element bow, in: Proceedings of the Transient Fuel Modelling Conference, Bournemouth, England, April 1978.
[256] A.S. Bain, A.W.L. Segal, J. Novak, Examination of Fuel Bundles Irradiated in Intermittent Dryout, AECL-5784, May 1977.
[257] G.I. Hadaller, G.H. Archinoff, E. Kohn, CANDU fuel bundle behaviour during degrading cooling conditions, in: Canadian Nuclear Association Conference, June 1983.
[258] E. Kohn, G.I. Hadaller, R.M. Sawala, G.H. Archinoff, S.L. Wadsworth, CANDU fuel deformation during degraded cooling (experimental results), in: Sixth Annual Conference of the Canadian Nuclear Society, Ottawa, Canada, June 3–4, 1985.
[259] K.R. Mayoh, Fuel channel high temperature transient program archive index, COG R&D Report COG-94-141, August 1995.
[260] J. Schenk, J. Whelan, Investigation of the thermal behaviour of a 37 element bundle in decay heat under degraded cooling conditions, COG R&D Report COG-91-228, July 1992.
[261] R.S. Dickson, A.I. Belov, M.D. Gauthier, R.T. Peplinskie, C.A. Buchanan, Fuel behaviour and fission-product release in hot-cell power-pulse tests, COG Report COG-03-2034, September 2004.
[262] O. Akalin, C. Blahnik, B. Phan, F. Rance, Fuel temperature escalation in severe accidents, in: Sixth Annual Conference of the Canadian Nuclear Society, Ottawa, Canada, June 3–4, 1985.
[263] E. Kohn, P.J. Fehrenbach, J.H. Lau, G.M. Archinoff, D.G. Hardy, A LOCA blowdown test of CANDU fuel elements, in: Sixth Annual Conference of the Canadian Nuclear Society, Ottawa, Canada, June 3–4, 1985.
[264] B.J. Lewis, L.W. Dickson, F.C. Iglesias, Contribution of Phebus FP to the knowledge of core melt progression and fission product release behaviour under severe accident conditions, in: Fourth Technical Phebus FP Seminar, Marseille, France, March 20–22, 2000.
[265] R.D. MacDonald, J.W. DeVaal, D.S. Cox, L.W. Dickson, M.G. Jonckheere, C.E. Ferris, N.A. Keller, S.L. Wadsworth, An in-reactor loss-of-coolant test with flow blockage and rewet, in: Proceedings of the Thermal Reactor Safety Meeting, Portland, Oregon, 1991 July, Also Released as an AECL Report AECL-10464, October 1991.
[266] J.W. DeVaal, N.K. Popov, R.D. MacDonald, L.W. Dickson, R.J. Dutton, D.S. Cox, M.G. Jonckheere, Post-test simulations of BTF-107: an in-reactor loss-of-coolant test with flow blockage and rewet, in: Proceedings of the Third International Conference on CANDU Fuel, Pembroke, Ontario, Canada, 1992 October, also released as AECL Report AECL-10758, March 1993.
[267] L.W. Dickson, P.H. Elder, J.W. DeVaal, J.D. Irish, A.R. Yamazaki, Preliminary results of the BTF-104 experiment: an in-reactor test of fuel behaviour and fission-product release and transport under LOCA/LOECC conditions, in: Proceedings of the Canadian Nuclear Society 1995 Annual Conference, Saskatoon, Saskatchewan, Canada, June 1995.
[268] L.W. Dickson, J.W. DeVaal, J.D. Irish, P.H. Elder, M.G. Jonckheere, A.R. Yamazaki, The BTF-104 experiment: an in-reactor test of fuel behaviour, and fission-product release and transport under LOCA/LOECC conditions, in: Proceedings of the Fourth International Conference on CANDU Fuel, Pembroke, Ontario, Canada, October 1995.
[269] R.S. Dickson, L.W. Dickson, Post-test analysis of the BTF-104 severe fuel damage experiment using the VICTORIA fission product transport code, in: Presented at Third OECD Specialist Meeting on Nuclear Aerosols in Reactor Safety, Cologne, Germany, June 15-18, 1998.
[270] J.W. DeVaal, J.D. Irish, L.W. Dickson, S.T. Craig, M.G. Jonckheere, L.R. Bourque, Preliminary results of the BTF-105A test: an in-reactor instrument development and fuel behaviour test, in: Proceedings of the Fifth International Conference on CANDU Fuel, Toronto, September 21–25, 1997.
[271] P.J. Valliant, J.D. Irish, S.T. Craig, Post-irradiation examination results from the BTF-105A LOCA/LOECC test, in: Proceedings of the Sixth International Conference on CANDU Fuel, Niagara Falls, Canada, September 26–29, 1999.
[272] J.D. Irish, S.T. Craig, L.R. Bourque, M.G. Jonckheere, G. Kyle, P.J. Valliant, L.W. Dickson, R.T. Peplinskie, Preliminary results of the BTF-105B experiment: an in-reactor test of fuel behaviour and fission-product release and transport under LOCA/LOECC conditions, in: Proceedings of the 19th Annual Conference of the Canadian Nuclear Society, Toronto, October 18–21, 1998.
[273] J.D. Irish, S.T. Craig, P.J. Valliant, Preliminary fission-product and post-irradiation examination results from the BTF-105B LOCA/LOECC test, in: Proceedings of the Sixth International Conference on CANDU Fuel, Niagara Falls, Canada, September 26–29, 1999.
[274] P.B. Middleton, R.C.K. Rock, S.L. Wadsworth, FACTAR 2.0 code validation, in: Fifth International Conference on CANDU Fuel, Toronto, Canada, 1997.
[275] D.H. Barber, Y. Parlatan, L.W. Dickson, B. Corse, M.H. Kaye, B.J. Lewis, W. Thompson, K. Colins, R.S. Dickson, Y. Hoang, R.J. Lemire, C.G. McLean, W.C. Muir, A. Popescu, B. Szpunar, S. Yatabe, SOURCE IST: fission product release code, in: Ninth International Conference on CANDU Fuel, Belleville, Ontario, Canada, 2005.
[276] L.W. Dickson, R.S. Dickson, R.J. Lemire, S. Sunder, SOPHAEROS-IST 2.0 validation: an update on the current status, in: CNS Sixth International Conference on Simulation Methods in Nuclear Engineering, Montreal, Québec, Canada, 2004.
[277] D.S. Cox, C.E.L. Hunt, Z. Liu, F.C. Iglesias, N.A. Keller, R.D. Barrand, R.F. O'Connor, A model for the release of low-volatility fission products in oxidizing conditions, in: Proceedings of the 12th Annual Conference Canadian Nuclear Society, Saskatoon, Saskatchewan, 1991.
[278] D.S. Cox, C.E.L. Hunt, Z. Liu, N.A. Keller, R.D. Barrand, R.F. O'Connor, F.C. Iglesias, Fission-product releases from UO_2 in air and inert conditions at 1700–2350 K: analysis of the MCE-1 experiment, in: Presented at the American Nuclear Society International Topical Meeting on the Safety of Thermal Reactors, Portland, Oregon, USA, July 21–25, 1991.
[279] D.S. Cox, Z. Liu, R.S. Dickson, P.H. Elder, Fission-product releases during post-irradiation annealing of high-burnup CANDU fuel, in: Proceedings of the Third International Conference on CANDU Fuel, Chalk River, Canada, October 4–8, 1992.
[280] D.S. Cox, Z. Liu, P.H. Elder, C.E.L. Hunt, V.I. Arimescu, Fission-product release kinetics from CANDU and LWR fuel during high-temperature steam oxidation experiments, in: Fission Gas Release and Fuel Rod Chemistry Related to Extended Burnup, IAEA-TECDOC-697, 1993.
[281] R.S. Dickson, Z. Liu, D.S. Cox, N.A. Keller, R.F. O'Connor, R.D. Barrand, Cesium release from CANDU fuel in argon, steam and air: the UCE-12 experiment, in: Proceedings of the 15th Annual Canadian Nuclear Society Conference, Montreal, Quebec, June 5–8, 1994.
[282] R.D. Barrand, R.S. Dickson, Z. Liu, D.D. Semeniuk, Release of fission products from CANDU fuel in air, steam and argon atmospheres at 1500–1900 °C: the HCE3 experiment, in: Proceedings of the Sixth International Conference on CANDU Fuel, Niagara Falls, Canada, September 26–29, 1999.
[283] M. Tayal, Nucl. Eng. Des. 116 (1989) 149–159.
[284] S.G. Xu, Z. Xu, S.D. Yu, M. Tayal, L. Lai, B. Wong, Bow code development-modeling of in-reactor bundle deformation, in: Ninth International Conference CANDU Fuel, Belleville, Ontario, September 19–21, 2005.
[285] M. Samaras, M. Victoria, W. Hoffelner, J. Nucl. Mater. 392 (2009) 286–291.